

WATOS: Efficient LLM Training Strategies and Architecture Co-exploration for Wafer-scale Chip

Huizheng Wang[†], Zichuan Wang[†], Hongbin Wang[†], Jingxiang Hou[†], Taiquan Wei[†], Chao Li[‡],
Yang Hu^{†✉}, Shouyi Yin^{†*}

[†]School of Integrated Circuits, BNRist, Tsinghua University, Beijing, China, 100084

[‡]School of Computer Science and Engineering, Shanghai Jiao Tong University, Shanghai, China, 200240

*Shanghai Artificial Intelligence Laboratory, Shanghai, China, 200433

✉Corresponding author, hu_yang@tsinghua.edu.cn

Abstract—Training large language models (LLMs) imposes extreme demands on computation, memory capacity, and interconnect bandwidth, driven by their ever-increasing parameter scales and intensive data movement. Wafer-scale integration offers a promising solution by densely integrating multiple single-die chips with high-speed die-to-die (D2D) interconnects. However, the limited wafer area necessitates trade-offs among compute, memory, and communication resources. Fully harnessing the potential of wafer-scale integration while mitigating its architectural constraints is essential for maximizing LLM training performance. This imposes significant challenges for the co-optimization of architecture and training strategies. Unfortunately, existing approaches all fall short in addressing these challenges.

To bridge the gap, we propose WATOS, a co-exploration framework for LLM training strategy and wafer-scale architecture. We first define a highly configurable hardware template designed to explore optimal architectural parameters for wafer-scale chips. Based on it, we capitalize on the high D2D bandwidth and fine-grained operation advantages inherent to wafer-scale chips to explore optimal parallelism and resource allocation strategies, effectively addressing the memory underutilization issues during LLM training. Compared to the state-of-the-art (SOTA) LLM training framework Megatron and Cerebras’ weight streaming wafer training strategy, WATOS can achieve an average overall throughput improvement of 2.74 \times and 1.53 \times across various LLM models, respectively. In addition, we leverage WATOS to reveal intriguing insights about wafer-scale architecture design with the training of LLM workloads.

I. INTRODUCTION

Large language models (LLMs) have emerged as pivotal components in advancing AI in recent years [19, 123]. Their success is primarily attributed to unprecedented model scales, which impose substantial demands on computation, bandwidth, and memory resources [139, 141]. Unfortunately, with the slowing of Moore’s Law [87] and the limited photomask size [150], monolithic devices increasingly struggle to provide the necessary transistor density and memory capacity to support LLM training efficiently [30, 70].

Wafer-scale chips (WSCs) [40], using advanced packaging technologies such as Chip-on-Wafer-on-Substrate (CoWoS) [44] to scale up the chip area, delivering a promising solution to overcome these limitations and enable continuous transistor integration. Currently, UCLA’s wafer-scale processor [102], wafer-scale GPU [103], Tesla Dojo [127], Cerebras WSE series [73, 74, 79] and TSMC SoW-X [121] have been

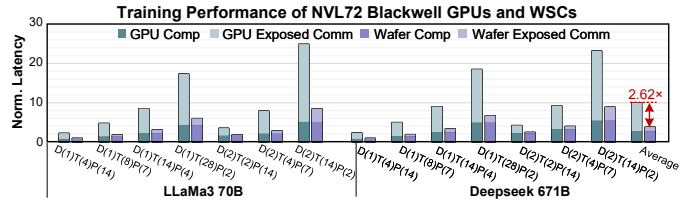


Fig. 1. Comparison of normalized training latency between NVL72 GB300 and WSCs under various parallelism configurations. The configuration D(1)T(4)P(14) indicates that there are 1/4/14 dies for DP/TP/PP dimension.

introduced. Compared to the most advanced GPUs [93] with high-speed rack-scale fabrics (i.e., NVLinks [96]), these WSCs can provide around 6 \times the inter-chip bandwidth and 5 \times lower link latency. Our characterization in Fig. 1 reveals that, under equivalent compute power, the 56-die WSC achieves a 2.62 \times reduction in effective communication latency compared with the state-of-the-art (SOTA) 56-GPU NVIDIA GB300 system [95] configured with NVL72. This result highlights the substantial potential of WSCs for LLM training.

However, unlike traditional ASIC designs [18, 56, 86, 136, 143], chiplet-based architectures [5, 106, 120, 147] or DGX-class systems [97, 124, 131], WSCs face a unique architectural challenge: the total physical area available for compute and memory resources is strictly limited by the wafer’s size, typically around 40,000 mm². This constraint imposes a fundamental trade-off: Expanding on-wafer memory capacity necessarily reduces the silicon budget available for compute resources, and vice versa.

Therefore, enabling efficient LLM training on WSCs demands tightly coordinated optimization along two fundamental levels: (1) Architecture level, where the system must be tailored to LLM workload characteristics, balancing compute and memory resources for optimal performance. **(2) Training strategy level**, which involves designing optimal parallelism to align with architectural constraints, efficiently distributing tasks to fully exploit the WSC’s capabilities.

However, upon re-examining existing works, we identify that the co-design of training strategies and architectural levels for LLM training remains largely unexplored. Most existing research continues to focus on single-level optimizations.

Isolated optimizations on training strategy level. Prior

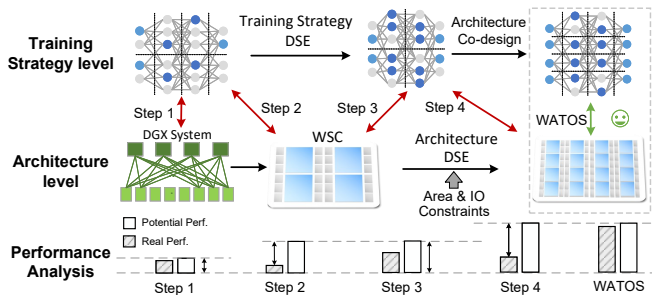


Fig. 2. Illustration of the training strategies and architecture co-design. The GPU system consists of 8 Blackwell Ultra GPUs, providing a total compute capacity of 40,000 TFLOPS, 2304 GB of HBM, 1.8 TB/s of NVLink interconnect bandwidth, and 8 TB/s of memory bandwidth. For fairness, the WSC is configured with equivalent compute power, as detailed in §V-C.

arts [43, 60, 90, 94, 122, 126] have proposed various training optimizations, such as auto parallelism, mixed precision [32, 85], offloading [168], compression [43], and recomputation [126], which significantly improve GPU training performance, as shown in the step 1 of Fig. 2. However, the performance ceiling is fundamentally constrained by the limited bandwidth of the board-level interconnect in DGX systems. Achieving higher performance urgently requires training strategies specifically designed for WSCs.

Isolated optimizations on architecture level. Several studies [7, 23, 102, 103, 114, 158] have attempted to explore wafer-level architectures, involving interconnect topologies [158], interconnect substrates [103], and chiplet design [7]. However, these works, on one hand, lack the collaborative optimizations with training strategies, leading to suboptimal performance, as step 2 in Fig. 2. For example, when applying Megatron’s parallel setup to train Llama2-30B on a WSC, we observe a 80% performance gap between real and potential performance. Therefore, to fully unlock the potential of hardware resources, it is critical to co-design training strategies with the architecture. As revealed in step 3&4 of Fig. 2, the absence of training strategy-architecture synergy results in the inability to fully leverage the WSC architecture’s potential. On the other hand, existing WSC designs often fail to thoroughly consider physical area constraints, thereby preventing the realization of an optimal wafer architecture design.

However, it is far from trivial to develop a co-design framework that integrates training strategy and architecture. It faces three key challenges: 1) The lack of configurable wafer-scale hardware templates for design space exploration (DSE). 2) The absence of systematic memory-centric training optimizations tailored to WSCs. 3) Naïve greedy co-design strategies are prone to getting trapped in local optima.

To address these challenges, in this paper, we develop a physical-constraints aware training strategy and architecture co-exploration framework, WATOS, as the step 5 in Fig. 2. Our contributions are summarized as follows:

1) Targeting WSCs, we design a highly configurable hardware template. Leveraging this template, WATOS systematically identifies and exploits latent co-optimization opportunities between **wafer architecture** and **training strategies**.

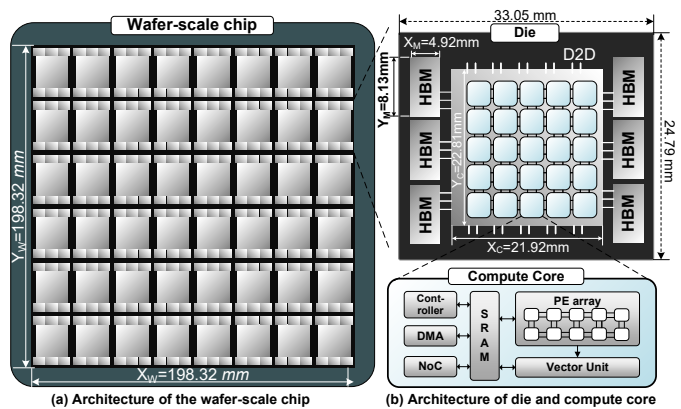


Fig. 3. Architecture of wafer-scale chips (WSCs).

These opportunities become particularly critical in the post-Moore era. To the best of our knowledge, this is **the first work** to enable such joint optimization.

2) To efficiently explore the co-design space, WATOS integrates the following key innovations: (1) An early-pruning central scheduler to accelerate the DSE process. (2) A globally coordinated memory-efficient recomputation (GCMR) strategy that maximizes memory savings while minimizing pipeline bubble overhead. (3) A global communication-cost aware resource placement and allocation strategy to reduce communication costs. (4) A genetic algorithm (GA)-based optimizer to accelerate convergence toward the global optimum.

3) Using WATOS, we uncover several intriguing insights for the WSC architecture and the LLM training: (1) With WATOS’ joint optimization, WSCs with moderate per-die DRAM capacity can achieve a balanced allocation of compute, communication, and memory resources, yielding near-optimal training throughput. (2) With tailored resource allocation and memory scheduling, smaller TP configurations on WSCs can realize better training performance than larger ones. (3) Enabled by our dedicated memory management strategies, efficient LLM training on WSCs demands not only high DRAM bandwidth but also ample communication bandwidth, making their balance crucial for optimal performance.

4) Compared to the SOTA LLM training systems and Cerebras wafer training strategy, WATOS’s co-optimized architecture and training strategies achieve an average performance gain of 2.74 \times and 1.53 \times , respectively.

II. BACKGROUND

A. Wafer-scale Chip (WSC)

WSCs integrate multiple functional dies using advanced packaging technologies like TSV [28, 51, 63], CoWoS [41, 44, 159], and RDL [38, 39, 64, 65]. There are two main approaches to wafer-scale integration: 1) Monolithic integration, where all compute dies and interconnects are fabricated directly on a single wafer substrate [6, 31, 73]. 2) Chiplet-based integration, where compute dies are fabricated separately and bonded to the wafer-scale interconnect [1, 102, 103, 120]. Given the latter offers greater flexibility, scalability, and yield,

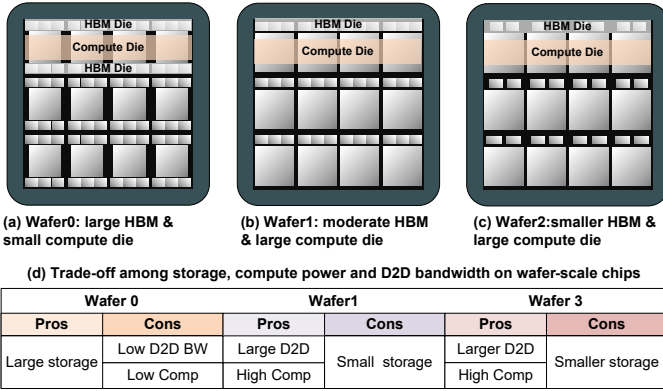


Fig. 4. Trade-off among storage, compute power and D2D bandwidth on WSC.

as individual dies can be independently optimized and tested before integration, this paper focuses on the chiplet-based WSC architecture.

Wafer-level architecture. As illustrated in Fig. 3, the WSC hardware template is structured into three hierarchies: wafer, die, and core. At the wafer level, a 2D mesh topology is deployed on the 198mm \times 198mm wafer to achieve efficient communication between adjacent dies, supporting modes including Die-to-Die and Die-to-HBM. This topology offers superior bandwidth and signal integrity compared to alternatives, making it the preferred choice for wafer-scale architectures.

Die & Core architecture. Each die integrates both computation and DRAM resources, unlike conventional chiplet designs that typically decouple these components [5, 88, 120, 128]. As depicted in Fig. 3, each die consists of multiple compute cores, a Network-on-Chip (NoC), HBM chiplets and peripheral D2D interfaces. The NoC adopts a 2D mesh topology, enabling low-latency communication across cores. At the core level, each core is managed by a local controller and communicates via the NoC and DMA engine. It comprises a shared SRAM, a PE array for GEMM operations, and a vector unit for scalar computation.

Configurable Hardware Template. Our hardware template offers a range of adjustable architectural parameters. These parameters include: 1) at the wafer level, compute die size (X_C, Y_C), DRAM die size (X_M, Y_M), the number of dies in horizontal (N_D^X , e.g., 8 in Fig. 3), vertical dimensions (N_D^Y , e.g., 6 in Fig. 3) along with DRAM/SRAM capacity, as well as NoC topologies. At the die level, compute units are configurable in core array dimensions and the number of MAC units per PE array. The PE microarchitecture and dataflow are derived from prior accelerator designs [9, 10, 33, 54, 61, 128, 137, 138, 140, 142, 145, 160].

B. Large Model Distributed Training

There are three primary parallel training methods: data parallelism (DP) [112, 117, 154], where each die stores the full model and synchronizes gradients across dataset shards; tensor parallelism (TP) [16, 122, 146], which partitions tensors along specific dimensions across dies; and pipeline parallelism (PP) [21, 45, 89], which splits the model into sequential stages

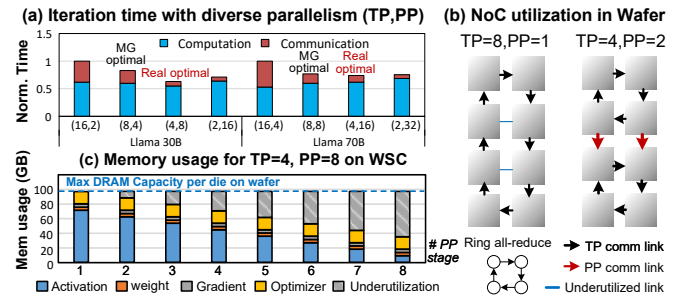


Fig. 5. Current LLM training parallelism framework is unsuitable for WSCs.

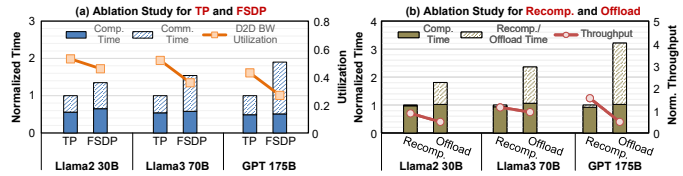


Fig. 6. Ablation Study for (a) FSDP and (b) Offloading. WSC is configured as §V-A with host-WSC PCIe 160GB/s [127].

executed in order. PP is often implemented using one-forward-one-backward (1F1B) schedule [21], which effectively reduces memory consumption compared to traditional PP strategies [45, 108]. As in Fig. 8 (a), the 1F1B schedule consists of three phases: warmup, steady and ending. For p stages and n micro-batches ($p=3, n=5$ in Fig. 8 (a)), a die at stage s first performs $p-s$ forward passes during warmup, then alternates $n-p+s$ forward and backward passes in the steady phase, and completes $p-s$ backward passes in the ending phase. However, 1F1B has imbalanced memory usage [126], as dies at the stage s must retain intermediate activations for $p-s$ micro-batches, as shown by the number of saved activation blocks in Fig. 8 (a).

Recently, bidirectional PP schedules [17, 72, 77] are proposed. However, these methods intensify memory pressure as model parameters are duplicated across stages. In addition, when $n > p$, these schedules often incur more pipeline bubbles than 1F1B. Moreover, DP also suffers from high memory overhead due to full model replication. Even advanced DP method like FSDP [166], which shards model states to reduce memory usage, perform poorly on WSCs due to heavy traffic of weights, gradients and optimizer states. As Fig. 6 (a) shows, such traffic congests the 2D-mesh NoC, causing a 20%–40% drop in bandwidth utilization compared to TP, which transmits activations only. **Thus, we focus on coordinating TP and PP under 1F1B scheduling to scale LLM training on WSCs.**

C. LLM Training System

Batching is widely adopted in modern LLM training to improve computation efficiency and accelerate convergence [91, 133, 134]. However, large batch sizes lead to excessive memory occupancy. To address this, training frameworks like Megatron-LM [122] and DeepSpeed [116] adopt memory optimization techniques such as mixed precision [4, 53, 85], offloading [110, 113, 117], and activation recomputation [8, 48, 107]. While effective in conventional systems, some of

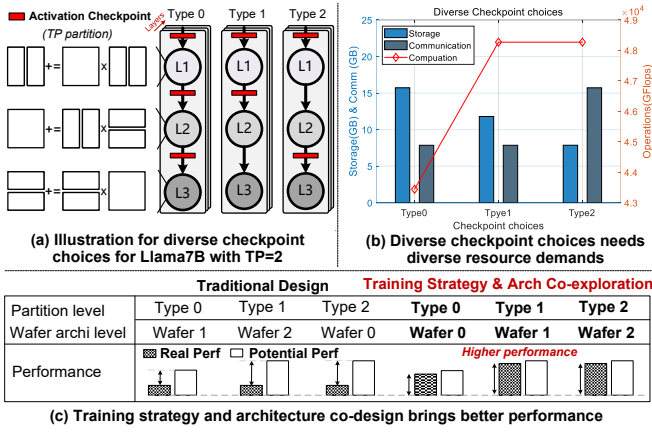


Fig. 7. Potential of training strategy and architecture co-design in WSCs.

these are ill-suited for WSCs. For example, compared to the immense computation capability and on-chip bandwidth of WSCs, limited bandwidth between host and WSC leads to severe computation stalls, making offloading impractical in wafer scenarios. In contrast, **activation recomputation is more well-suited to WSCs, as it reduces memory usage without external data transfer.** As shown in Fig. 6 (b), compared with recomputation, offloading incurs substantially higher overhead, resulting in an average $2.2\times$ increase in wall-time latency. Despite the advantage, the recomputation alters the memory-to-compute ratio, reshaping hardware resource demands. This calls for a co-design of training strategies and wafer architecture, an aspect that remains unexplored in existing works.

III. MOTIVATION

A. Problems in LLM Training on WSCs

While existing training systems have recognized the resource-intensive characteristic of LLM training and adopted hybrid parallelism to address it, several key problems remain:

First, existing systems often fail to achieve optimal parallelism on WSCs due to a lack of consideration for the underlying interconnect topology. To demonstrate this, we conducted experiments using Llama-30B/70B models across 32 and 64 dies on a WSC. The compute die configuration is detailed in §V-B. Based on the model configurations, we derived the optimal parallelism settings recommended by the Megatron framework [94] (MG-optimal), which suggests (TP, PP) = (8, 4) for 32 dies and (8, 8) for 64 dies. We then deployed these settings on the WSC to evaluate actual performance. As shown in Fig. 5 (a), on the WSC, configurations of (4, 8) for 32 dies and (4, 16) for 64 dies outperform the MG-optimal settings. This discrepancy arises from Megatron’s ignorance of the WSC’s 2D mesh interconnect. As depicted in Fig. 5 (b), naively setting TP = 8 leads to link under-utilization during Ring All-Reduce, affecting communication efficiency. In contrast, TP=4 with PP=2 achieves more balanced link utilization and better overall performance.

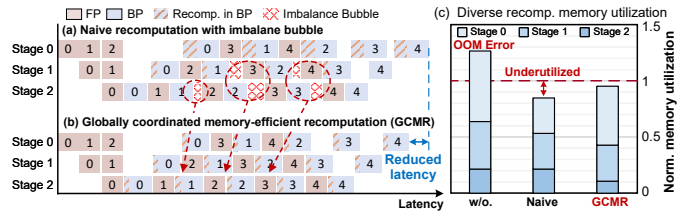


Fig. 8. Illustration of the imbalance bubble caused by naive recomputation and its underutilized memory.

Second, imbalanced memory usage incurred by large PP leads to underutilized DRAM resources on WSCs. Fig. 5 (c) shows peak DRAM usage during Llama-30B training with TP=4 and PP=8 on a WSC, where each die is equipped with 96 GB of DRAM (detailed in §V-B). The results reveal pronounced disparities in average DRAM utilization among dies on the WSC. Dies at the early stages of the pipeline exhibit much higher memory pressure than those at the tail. This skew is caused by checkpointed intermediate activations, which account for over 70% of total memory usage.

B. Trade-off among Compute-Memory-Comm on WSCs

LLM training imposes substantial demands on compute, memory, and communication resources. WSCs enable large-scale integration for diverse function dies, but remain constrained by the physical wafer size, which provide around 40,000 mm² of usable area on a 12-inch wafer. **This architecture feature highlights a trade-off among on-wafer compute, memory, and interconnect resources.**

Figs. 4 (a–c) depicts three WSC configurations with varying DRAM chiplet counts. **Wafer 0** places six DRAM chiplets on both sides of the compute die, maximizing memory capacity for storing large models and checkpoints. **Wafer 1** reduces DRAM to three chiplets on one side, reallocating area to enlarge the compute die and improve both compute capability and D2D bandwidth. **Wafer 2** retains the Wafer 1’s compute-die size but further reduces DRAM, freeing more peripheral IO to enhance D2D bandwidth. Fig. 4 (d) summarizes the inherent architecture trade-off. (1) Increasing DRAM capacity reduces space available for compute dies, in turn lowering compute density. (2) Given the fixed number of compute-die interconnect interfaces, allocating more interfaces to DRAM reduces the bandwidth available for D2D links.

C. Untapped Potential of Training Strategy & WSC Co-design

Fig. 7 (a) illustrates three checkpoint (i.e., recomputation) strategies (Type 0-2) applied to a computation graph with three operators (L1-L3) with TP=2, where each operator represents the corresponding operation across all layers. Type 0 stores all activation checkpoints without recomputation. Type 1 recomputes outputs of operator L2, while Type 2 recomputes L1’s output. Due to operator-specific tensor partitioning, each strategy incurs distinct compute, storage, and communication demands. As depicted in Fig. 7 (b), Type 0 has the highest storage cost but minimal computation overhead, as it avoids recomputation entirely. In contrast, Type 1 and Type 2 incur

higher compute overheads, but differ in storage and communication footprints based on which activations are recomputed.

These distinct training strategies impose specific demands for on-wafer resource allocation, underscoring the co-design of training strategies and architecture. As depicted in Fig. 7(c), traditional designs often focus solely on strategy-level optimizations, while neglecting architectural adaptation, leading to sub-optimal real performance. By contrast, co-design leverages dominant tensor partitioning and recomputation patterns to proactively tailor wafer architectures to the needs of typical training workloads, seeking enhanced overall performance.

Unfortunately, existing DSE frameworks almost fail to leverage the co-optimization of training strategies and architecture, let alone account for wafer-level architectural constraints. Table I summarizes their features. Timeloop [105] focuses on die-level mapping exploration and architecture optimization, while Hecaton [46] and Gemini extend to the chiplet scale. DFModel [59], Calculon [47] and Bpipe [57] explore optimal training strategy or scheduling on GPU clusters, but none of these works consider the unique constraints of WSCs. Recent works like WSC-LLM [156] and PD [158] realize WSC constraints, but one focuses on inference and the other on topology optimization, lacking a comprehensive training strategy. They overlook custom training optimizations for recomputation and checkpoint overheads, which motivates the development of WATOS.

IV. WATOS FRAMEWORK

As depicted in the left of Fig. 9, WATOS takes architecture parameter candidates, LLM model configs, and training datasets as inputs. Considering wafer area constraints, architecture parameter candidates are derived from arbitrary combinations of configurable parameters (as in §II-A). All architectural candidates are first exhaustively explored in an *Enumerator*, then sent to the *Co-exploration Engine* to determine the achievable optimal LLM training performance on WSCs.

Overall workflow. As shown in the right part of Fig. 9, the central scheduler first iterates through feasible TP and PP sizes, and preliminarily allocates resources across pipeline stages. Then, the recomputation scheduler prevents memory overflow by selectively recomputing activations with minimal latency overhead. Next, the memory scheduler optimizes on-wafer memory usage by topology-aware resource placement and fine-grained DRAM allocation. Further, the global optimizer applies genetic algorithms to search the remaining design space and identify optimal configurations. Finally, the execution engines generate detailed implementation plans, invoke the *Evaluator* to assess performance, and return results to the central scheduler for the next exploration round.

A. Central Scheduler

Given the trade-off between memory, computation, and communication on WSCs, we prioritize model parallelism within a single wafer, requiring careful TP and PP partitioning. This presents two challenges: determining the optimal TP/PP

TABLE I
SUMMARY OF FRAMEWORKS (CO-DE: CO-DESIGN, OPT: OPTIMIZATION)

Framework	HW Optimization			Recomp aware	WSC Physical	WSC Co-de	Opt level
	Comp	Mem	D2D				
Timeloop [105]	✓	×	×	×	×	×	die
Hecaton [46]	✓	✓	✓	×	×	×	chiplet
Gemini [5]	✓	✓	✓	×	×	×	chiplet
DFModel [59]	✓	×	×	×	×	×	cluster
Calculon [47]	✓	✓	×	✓	×	×	cluster
BPipe [57]	✓	✓	✓	×	×	×	cluster
FRED [114]	✓	×	✓	×	×	✓	wafer
PD [158]	✓	×	✓	×	✓	✓	wafer
WSC-LLM[156]	Low	×	×	×	✓	✓	wafer
WATOS	✓	✓	✓	✓	✓	✓	wafer

ratio while considering architectural constraints, and managing activation checkpoints to prevent out-of-memory (OOM) errors

To this end, we propose Alg. 1, which systematically optimizes resource partitioning for TP and PP. Our optimization is based on the premise that training data consists of four parts: model weights, gradients, optimizer states, and activation checkpoints. The first three, collectively referred to as *modelP*, are essential and must be retained throughout the training process, while activation checkpoints are optional and can be regenerated through recomputation. Thus, minimal model-parallel units must fit *modelP* in their aggregate memory.

Given a model M , model-parallel dies MP , per-die DRAM capacity C , workload W , the central scheduler first checks if *modelP* fits within the max aggregate memory capacity of the MP. If not, it will directly prune the parallelism candidate (line 1, 2). It then iterates over all feasible TP and PP sizes, for each mp within the MP (line 4), ensuring the TP instance consists of an even number of dies to meet the 2D-mesh topology communication requirements. Once the TP and PP are determined, the algorithm checks if the checkpoint storage requirement is met (line 5). For failed configurations, it delegates them to downstream schedulers, which employ recomputation and memory allocation to ensure compliance (line 6). Finally, the algorithm enumerates all possible TP partition strategies (line 7, detailed in §IV-E) to identify the max achievable throughput for each configuration, updating the current configuration if a better record is found (line 8).

B. Recomputation Scheduler

In §IV-A, we obtain the parallel configuration (TP_Config, PP_Config) that can accommodate the *modelP* with partial activation checkpoints. The remaining checkpoints exceeding on-wafer memory capacity can result in OOM errors that interrupt the training process. To address this limitation, recomputing these checkpoints enables training to proceed within the given memory constraints. However, as shown in Fig. 8 (b)(c), the naive recomputation strategy not only introduces pipeline bubbles but also underutilizes memory, thereby incurring additional computation overhead and degraded training throughput.

To this end, we propose a globally coordinated memory-efficient recomputation (GCMR) strategy, as outlined in Alg.

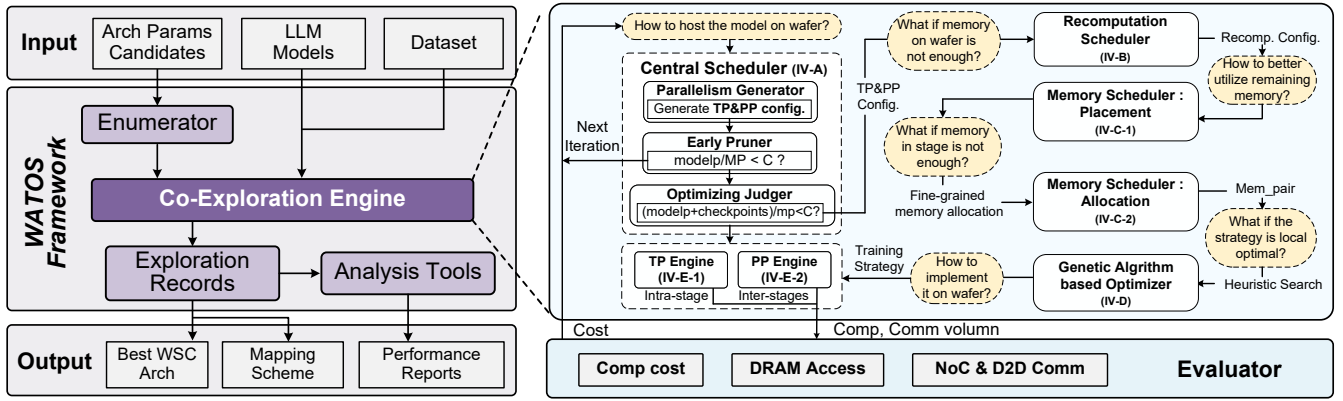


Fig. 9. The proposed WATOS framework for LLM training and wafer-scale architecture co-exploration.

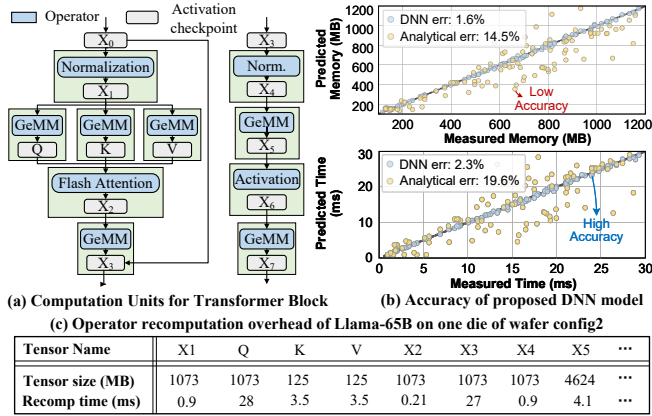


Fig. 10. Recomputation preparation for LLM models.

2. In contrast to the naive recomputation strategy depicted in Fig. 8 (a), the GCMR strategy takes into account the DRAM capacity across the entire WSC. It employs a global balanced recomputation strategy that minimizes the bubble while maximizing memory utilization, as demonstrated in Fig. 8 (b). Notably, the memory imbalance introduced by 1F1B pipeline may still lead to checkpoint overflows in early stages, like the stage0 and stage1 in Fig. 8 (c). Therefore, after generating the recomputation configuration $Recomp_config$, the GCMR identifies stages that are susceptible to such imbalance as Senders and those with sufficient memory as Helpers. The Helpers can receive the overflowing checkpoints from the Senders, thus balancing memory usage across the pipeline.

Given that most LLMs are based on the Transformer architecture, we begin with decomposing the computation into a set of fundamental operator units according to the Transformer graph, as shown in Fig. 10 (a). Each operator is annotated with its computation type as well as the associated checkpoint requirements, enabling fine-grained recomputation scheduling. We further incorporate the SOTA FlashAttention [13] mechanism as a specialized operator to capture its distinct performance and memory characteristics. To cover all possible setups, we train a DNN model to predict the execution latency and memory footprint of each operator, based on two key considerations: 1) Despite their precision, cycle-accurate

Algorithm 1: Early Pruning-based Central Scheduler

Input: Model M , die limit for MP MP , Die memory capacity C , Workload W , TP split strategy S

Output: OptimalConfig

```

1 if  $W.modelP/MP > C$  then
2   Prune(Candidate);
3 else
4   for  $tp \cdot pp == mp \in [1, MP]$  do
5     if  $(W.modelP + W.checkpoints)/mp > C$  then
6       DownstreamSchedulers(tp, pp)
7     for  $s \in S$  do
8       OptimalConfig  $\leftarrow \text{argmax}(test(W, tp, pp, s))$ 

```

simulators often require minutes to hours per run, making them impractical for large-scale performance evaluation. 2) Analytical models, on the other hand, fail to capture complex factors such as alignment overheads and multi-level memory effects, resulting in limited prediction accuracy. As depicted in Fig. 10 (b), DNN-based prediction can realize up to 17.3% higher accuracy over the analytical scheme. 3) Numerous simulator works have validated the feasibility of using DNNs, with prediction error remaining within a controllable range [58, 104, 156]. Therefore, we adopt a DNN model to predict the execution latency and memory footprint of each operator under different batch sizes and wafer-scale hardware configurations. The collective communication overhead of recomputed tensors between adjacent operators is estimated through the α - β model [130] as Eq. (1), where α represents link latency and β denotes the communication size of All-Reduce. This profiling is conducted offline and produces an operator-level performance lookup table for iterative process, as depicted in Fig. 10 (c).

$$t_{comm} = \alpha + \beta/BW, \quad \beta = 2 \cdot (TP - 1)/TP \cdot BSH \quad (1)$$

Based on the computation and memory characteristics of fundamental LLM operators, GCMR performs dynamic programming to accelerate the search for the optimal recomputation strategy. It begins from the last pipeline stage, incrementally allocating memory and querying the profile for latency

Algorithm 2: The Proposed GCMR Strategy

Input: TP Config, PP Config, Workload \mathbf{W}
Output: RecompConfig \mathcal{R} , SenderSet \mathcal{S} , HelperSet \mathcal{H}

```

1  $P \leftarrow \text{RecompProfiling}(pp, tp, \mathbf{W});$ 
2 for  $t = pp - 1 : 0$  do
3   for  $m = 0 : (pp - t) * C$  do
4      $t_{max} \leftarrow \max(T[t + 1, m - m_t], B_t + 2F_t - P(m_t));$ 
5      $T[t, m] \leftarrow \min_{m_t} (t_{max}), \text{Mem}[t, m] \leftarrow \underset{m_t}{\text{argmin}} (t_{max});$ 
6 for  $t = 0 : pp - 1$  do
7    $M[t] \leftarrow \text{Mem}[t, pp \cdot C - \sum_{i=0}^{t-1} M[i]], \mathcal{R}[t] \leftarrow P(M[t]);$ 
8   if  $M[t] > C$  then
9      $\mathcal{S}.append(\text{stage}_t);$ 
10  else
11     $\mathcal{H}.append(\text{stage}_t);$ 
12  $\mathcal{S}, \mathcal{H} \leftarrow \text{DescendSort}(\mathcal{S}, \mathcal{H});$ 
13 while  $\mathcal{H} \neq \emptyset$  do
14    $\text{Mem\_pair}(\mathcal{S}.pop(), \mathcal{H}.pop());$ 

```

and recomputation candidates, recursively incorporates preceding stages. After analyzing all stages, the algorithm identifies the optimal configuration by minimizing the maximum stage-execution time (line 2–5). Finally, the recomputation configurations along with memory footprints for each stage are generated (line 6–8). In this way, the GCMR achieves maximal global memory efficiency at minimal recomputation cost.

Moreover, lines 9–11 identify Senders and Helpers by examining the post-recompute memory footprint of each stage. Specifically, stages exceeding per-die memory capacity are marked as *Sender* for *checkpoints* offloading (lines 8,9), while others serve as *Helper* to receive the checkpoints (line 10,11). The algorithm then sorts the Sender and Helper sets by memory pressure and available memory (line 12) and invokes the Mem_pair procedure to pair memory-constrained Senders with memory-rich Helpers (lines 13,14). This pairing offloads the activation checkpoint from high-pressure stages to memory-rich stages, effectively balancing memory usage across the pipeline. **Notably, the offloading occurs across dies on a wafer, rather than off-wafer to external memory.**

C. Memory Scheduler

1. Optimal Resource Placement Strategy. In § IV-B, we investigate the memory-efficient recomputation configurations, along with the construction of the Mem_pair set. This pairing enables offloading checkpoints from the Sender to the DRAM chiplets of the Helper. However, due to characteristics of the 2D-mesh topology on wafer-scale chips, it is also necessary to determine the optimal placement of each instance.

Fig. 11 illustrates two resource placement strategies for an 8 stage pipeline with designated Mem_pair configurations ($S1, S8$) and ($S2, S7$). The pipeline stages are arranged linearly from $S1$ to $S8$, with activation checkpoint balance paths identified between the corresponding Mem_pairs. As can be seen, the conventional left-to-right, upper-to-bottom resource placement strategy results in long communication paths between Mem_pair stages, with an average of 6 hops.

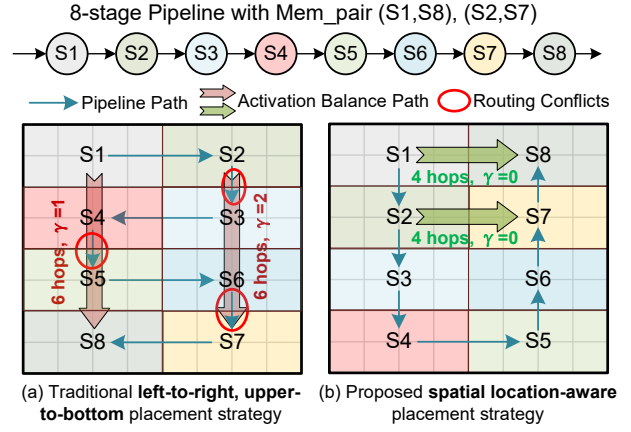


Fig. 11. Comparisons of different resource placement strategies.

In contrast, our proposed spatial location-aware placement approach strategically co-locates Mem_pair stages, significantly reducing the communication cost by shortening the path length from 6 hops to 4 hops. Moreover, when considering the overall communication hops, including those along the pipeline path, our strategy achieves a 30% reduction in total hop count.

Since the activation checkpoint transfer occurs from Sender instances to Helper instances, our objective is to minimize the total distance between each Sender instance and its Helper instance, while avoiding overlapping transmission paths with the pipeline paths. To achieve this, we adopt a globally location-aware placement strategy that preserves the critical path of the pipeline, while minimizing the transmission distance between Mem_pair stages. If multiple placement schemes exist, we select the one that minimizes the total communication cost. The selection is formalized as Eq. (2),

$$\begin{aligned}
 GlobalCost = \min & \left(\sum_{i=0}^{PP-1} Dist(S_i, S_{i+1}) \cdot Comm_{PP}(S_i, S_{i+1}) \right. \\
 & \left. + \sum_{(s,h) \in Mem_pairs} Dist(S_s, S_h) \cdot Comm_{pair}(S_s, S_h) \cdot (1 + \gamma) \right), \quad (2)
 \end{aligned}$$

where S_i denotes the center position of the pipeline stage, $i \in [0, PP - 1]$. $Comm_{PP}$ and $Comm_{pair}$ represent the pipeline and checkpoint transfer communication workload respectively, which are used as weights for distance. $Dist$ refers to the shortest path between the two pipeline stages. In cases where multiple shortest paths exist, all such paths are enumerated. To take routing conflicts into account of placement, the conflict factor γ is introduced, which stands for the number of conflict links between activation balance paths and existing pipeline paths. Paths with conflicts will be punished by $1 + \gamma$ in $GlobalCost$.

2. Location-aware DRAM capacity allocation. WSCs feature high D2D bandwidth, typically exceeding DRAM access bandwidth. This means that, cross-die DRAM read and write operations are limited by DRAM bandwidth rather than D2D bandwidth. Leveraging this advantage of the wafer-scale architecture, the extensive inter-die transfer of checkpoints can be overlapped by its DRAM access, allowing us to fully utilize

Algorithm 3: Location-aware DRAM Allocation Strategy

Input: Sender set \mathcal{S} , Helper set \mathcal{H}
Output: Memory pair set $\mathcal{A} = \{A_1, \dots, A_k\}$

```

1 for  $S_i \in \mathcal{S}$  do
2    $Q \leftarrow \text{sort}(\text{GlobalCost}(S_i, \mathcal{H}));$ 
3    $A_i \leftarrow \emptyset;$ 
4   while  $S_i.\text{OverflowMemory} > 0$  do
5      $d' \leftarrow Q.\text{pop}(); A_i.\text{append}(d');$ 
6     if  $d'.\text{capacity} > S_i.\text{OverflowMemory}$  then
7        $d'.\text{capacity} -= S_i.\text{OverflowMemory};$ 
8        $Q.\text{insert}(d');$ 
9     else
10       $S_i.\text{OverflowMemory} -= d'.\text{capacity};$ 

```

all DRAM resources on the wafer for the activation checkpoint storage, to achieve higher performance of LLM training.

As depicted in Alg. 3, we implement an location-aware DRAM allocation strategy for handling overflow checkpoints, to minimize the additional D2D transmission overhead. Given the Sender set \mathcal{S} , the Helper set \mathcal{H} , the algorithm finds the optimal DRAM destination for each Sender’s checkpoint. The algorithm first identifies the associated Helpers for each Sender without additional communication cost to form a priority queue Q , based on the existence of short transmission paths between their respective positions (line 2). For example, in Fig.10 (b), DRAMs within S2, S8 and S7 occupy top positions in the queue Q of S_1 . Subsequently, an empty Mem_pair A_i is initialized (line 3), and the algorithm iteratively allocates DRAM resources to the Sender S_i . The capacity of DRAMs of Helper is reduced by the portion utilized during the allocation process (line 5-7). After calculating the remaining capacity, the DRAM unit is reinserted into the queue Q (line 7-9), which is dynamically reprioritized to guide subsequent allocations. The allocation loop continues until the entire checkpoint requirement of S_i is met. Notably, the Alg. 3 does not conflict with the optimization in IV-C-1, but rather builds upon it to execute a fine-grained DRAM allocation strategy.

D. Global Optimizer

§IV-B and §IV-C present the optimal recomputation configuration and DRAM allocation strategy, respectively. However, maximizing memory utilization alone cannot guarantee full overlap of recomputation bubbles. The greedy strategy may fail to pair each Sender with the lowest-cost Helper, leading to local optima, as blue path in Fig. 12. To overcome this limitation, we employ a genetic algorithm (GA) [35], which can identify global optima within vast solution spaces based on evolutionary principles [119].

By integrating GA with customized operators, WATOS can thoroughly explore the design space toward near-optimal solutions. Specifically, given Recomp_config \mathcal{R} , Mem_pair \mathcal{A} and placement strategy, we develop five GA operators to facilitate the exploration process, as Op1-Op5 in Fig. 12:

Op1 \mathcal{R} variation: Randomly enable or disable recomputation for an operator while satisfying DRAM capacity.

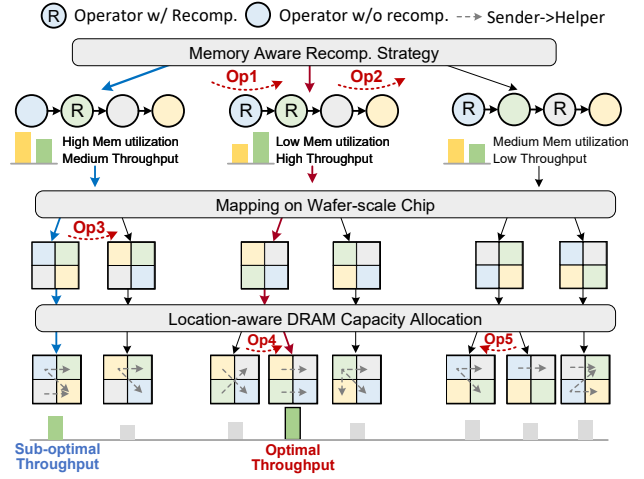


Fig. 12. Overview of genetic algorithm-based global optimizer.

Op2 \mathcal{R} crossover: Swap recomputation configurations between two randomly selected pipeline stages beyond a chosen backward operator.

Op3 Placement variation: Swap the physical positions of two randomly chosen stages on the wafer-scale chip.

Op4 \mathcal{A} variation: Modify the Mem_pair of a Sender by adding the lowest-cost Helper or removing part of a randomly selected Helper, while fulfilling the storage constraints.

Op5 \mathcal{A} crossover: Exchange Mem_pairs between two randomly selected Senders.

With these operators, mutations and crossover are introduced to generate new configurations. Then, a fitness function, defined as $t_{max} \times \text{GlobalCost}$, evaluates performance, and configurations are probabilistically eliminated to keep the search tractable. Crucially, these operators enable any feasible configuration to evolve into another through valid transformations. For instance, as depicted in Fig. 12, Op1 can introduce additional recomputation into the initial recomp_config, improving pipeline overlap at the expense of minor DRAM utilization. Then Op4 adjust Mem_pairs obtained from the greedy strategy, sacrificing the local optimum to reach global optima as red path in Fig. 12. Therefore, the Global Optimizer ensures that any point within the design space of WSC can be reached from any other point, thereby guaranteeing comprehensive exploration and yielding global optimal solutions.

E. TP & PP Execution Engines

To efficiently execute LLM operators on wafers, workloads must be partitioned and mapped across dies and cores. As shown in Fig. 13, a GEMM operator can be partitioned along four dimensions: batch size (B), sequence length (S), hidden size (H), and the reduction dimension (K). WATOS employs a two-level allocation strategy: Intra-stage allocation (§IV-E-1) and Inter-stage allocation (§IV-E-2).

1. TP Engine. Initially, the TP engine decomposes computation into die-level sub-computation tasks. Once receiving a sub-computation task, each die partitions it into basic computation tiles (e.g., along B, S, H, K) sized to fit within

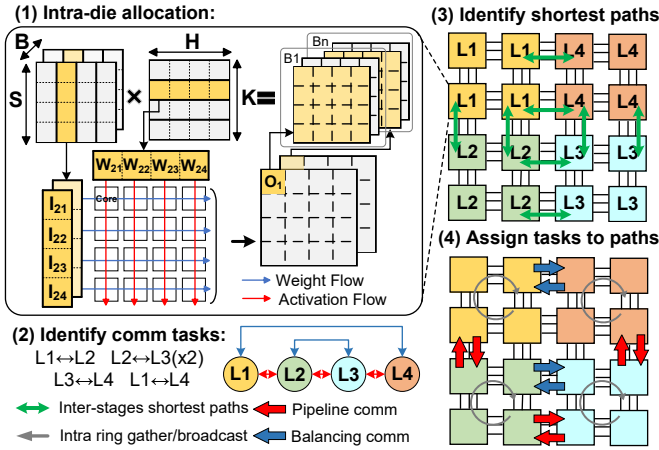


Fig. 13. Overview of TP&PP execution engine.

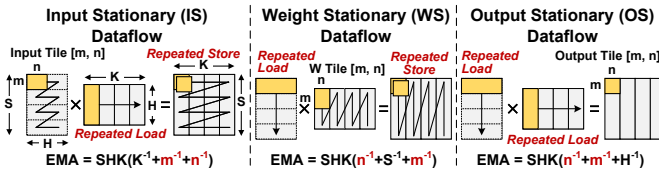


Fig. 14. Hybrid dataflows and EMA analysis using a $m \times n$ MAC array.

a single core’s SRAM. These tiles are then mapped and executed. As depicted in Fig. 13 (1), the TP Engine first partitions along the K dimension and assigns the sub-task to a die, which further partitions along S and H . Tiles are then mapped following an output-stationary (OS) dataflow and executed iteratively. However, OS may not fully maximize SRAM reuse, increasing system overhead. To address this, we further incorporate three additional dataflows: weight-stationary (WS), input-stationary (IS), and row-stationary (RS) [10]. Among them, RS is specifically designed for convolution operators. Apart from RS, the variations of OS, WS, and IS do not change the computational workload but alter the external memory access (EMA), as illustrated in Fig. 14, leading to differences in latency and energy consumption. Consequently, our intra-die dataflow adopts a hybrid design that dynamically selects the most suitable dataflow based on the operator type and EMA characteristics under different workloads. Upon completion of the computation, we implement all-gather and all-reduce operations in the TP process using the bidirectional ring algorithm [170], which aligns well with the 2D-mesh topology of WSCs. The TP engine can also be configured to explore other intra-stage communication mechanisms such as Multitree [42]. Overall, the TP engine provides a robust approach to dynamically optimize intra-stage computation and communication, guaranteeing an efficient training process.

2. PP Engine. Inter-stage communication is the major bottleneck in chiplet-based WSCs [120]. To mitigate contention from many-to-many communication, we adopt the following strategy for inter-stage communication, as shown in Fig. 13: Firstly, all inter-stage communication tasks, including pipeline data transfer between adjacent stages and activation balancing

TABLE II
PARAMETERS OF FOUR REPRESENTATIVE HARDWARE CONFIGURATIONS

Config. Type	Config 1	Config 2	Config 3	Config 4
#Die num	64	56	56	48
#Die in X,Y-dim	(8, 8)	(7, 8)	(7, 8)	(6, 8)
Comp Power	512	708	708	708
DRAM Bandwidth	1TB/s	1.5TB/s	2TB/s	2.5TB/s
DRAM per die	48GB	64GB	70GB	96GB
D2D Bandwidth	4.5TB/s	4.5TB/s	4TB/s	3.5TB/s

between senders and helpers, are identified. The shortest paths between corresponding stages are then determined. Subsequently, we allocate these communication tasks to links in order of size. In the allocation process, we prioritize unused links by giving a punishment factor to occupied links, and consequently avoid contention. As shown in Fig. 13, pipeline and activation balancing communications are overlapped as they occupy different links. Once the inter-stage communication cost determined, we can derive the execution time for a pipeline iteration based on the TP engine’s execution strategy.

F. Evaluator

The evaluator of the WATOS framework is built upon Astrasim [152], an efficient and widely adopted simulator to model distributed parallel execution. Our *Execution Engines* serves as the interface for global performance evaluation. To realize this, we introduce two significant efforts on Astrasim.

First, we extend ASTRA-sim by integrating detailed modeling of memory usage, computation, and communication overheads for key LLM operators. Additionally, we incorporate a DRAM chiplet capacity model to capture the on-die memory constraints. These enhancements enable memory-aware scheduling simulations, allowing Astrasim to more accurately reflect the resource consumption on WSCs.

Secondly, to enable rapid simulations, we pre-build a mapping lookup table offline by profiling optimal intra-die mapping strategies for representative configurations, including different models, sequence lengths, and batch sizes. For each case, we log key metrics such as latency, DRAM access volume, and communication overhead. During WATOS’s on-line execution, the table is accessed in a read-only manner with negligible overhead. The feasibility of this approach is supported by numerous works [49], showing the error of precomputed results remains within an acceptable range.

V. EVALUATION

A. Experiment Setup

Basic Hardware Configurations. To support wafer-scale architecture exploration, we configure the compute die parameters based on the setup illustrated in Fig. 3. The compute die have two configurations: (1) $21.92\text{mm} \times 22.81\text{mm}$ with a 16×16 array of Dojo-style cores, and (2) $25.5\text{mm} \times 25.2\text{mm}$ with an 18×18 core array. They are manufactured using TSMC’s 7 nm process technology and operates at a frequency of 2 GHz [127]. The edge of the compute die provides a total interconnect bandwidth of 12 TB/s across four directions. Each

core delivers a computational power of 2.04 FP16 TFLOPS and features 1.25 MB of SRAM.

Architectural DSE. In this study, we perform an architectural DSE of WSCs based on the compute chips. Each chip can integrate a varying number of DRAM chiplets, enabling different trade-offs in compute capability, memory capacity, and bandwidth. This exploration aims to demonstrate the advantages of WATOS and to provide deeper insights into the resource trade-offs on WSCs. Table II summarizes four representative wafer-scale configurations generated by the proposed enumerator, which serve as the basis for our DSE.

DSE Configurations. We evaluate WATOS on Intel Xeon Gold 6448H with 32 cores per socket. The runtime of the global optimizer is 0.274s for 100 exploration steps. Beyond runtime, we observe that the selection strategy inherently introduces a trade-off between exploration steps and final performance: 1) The elitist strategy selects only the fittest individuals, leading to fast convergence but often suboptimal performance. 2) Binary tournament selection preserves greater diversity, enabling better performance at the cost of slower convergence. We introduce ω as an interface to control the proportion of elitism. Fig. 24 (b) illustrates the impact of varying ω on both the convergence speed and the final performance.

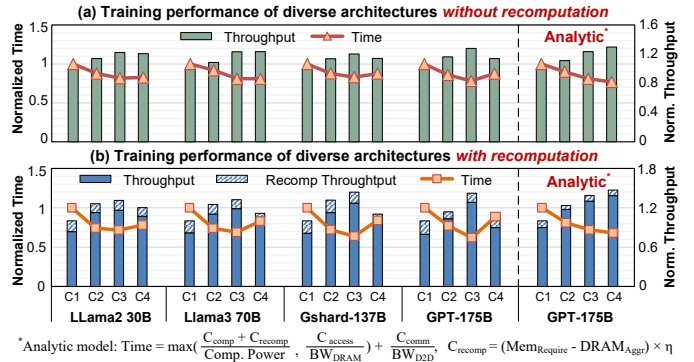
Workloads. We choose a series of models from 30B to 671B for our experiments, including dense models Llama2-30B [134], Llama3-70B [83], GPT-175B [3] and MoE models Gshard-137B [66] and Deepseek-v3 [17]. We adopt mixed precision training, with FP16 for weights and activations, and FP32 for Adam optimizers.

Metrics. To evaluate system performance, we adopt iteration time and throughput as metrics. Iteration time measures the latency of one forward and backward pass, while throughput denotes floating-point operations per second. All results are normalized to the lowest-performing configuration (value = 1). As recomputation may increase throughput without improving performance due to additional computation, we break down throughput results for all configurations using recomputation.

B. Architectural Design Space Exploration

As recomputation is critical in improving memory efficiency during training, a viable WSC must perform robustly under both recomputation and non-recomputation scenarios. Fig. 15 shows results of four feasible WSC architectures across representative LLM models, covering variations in sequence length and batch size for generalizable evaluation. Config 3 consistently achieves the best performance, demonstrating adaptability to diverse models and workloads, and emerging as the universal optimal WSC. These results suggest that a WSC with moderate per-die DRAM capacity and high compute density can effectively balance compute, memory, and communication demand during LLM training. In contrast, architectures with excessively large or small per-die DRAM suffer from imbalanced utilization and degraded performance.

The comparison between Config 2 and Config 4 shows that Config 4 performs better without recomputation, whereas Config 2 excels when recomputation is enabled. This shift



*Analytic model: $\text{Time} = \max\left(\frac{C_{\text{comp}} + C_{\text{recomp}}}{\text{Comp. Power}}, \frac{C_{\text{access}}}{\text{BW}_{\text{DRAM}}}\right) + \frac{C_{\text{comm}}}{\text{BW}_{\text{D2D}}}$, $C_{\text{recomp}} = (\text{Mem}_{\text{Require}} - \text{DRAM}_{\text{Ager}}) \times \eta$
 Fig. 15. Performance comparison for configs 1-4 on Llama2 30B, Llama3-70B, Gshard-137B, GPT-175B (a) w/o recomputation (b) w/ recomputation. Analytic model for DSE optimum only; idealized results not comparable.

stems from recomputation increasing compute demand while reducing DRAM requirements. As a result, Config 2’s higher compute density becomes beneficial under recomputation, but leads to performance degradation in non-recomputation scenarios. *This observation underscores that compute density, along with DRAM bandwidth and capacity, are key determinants of performance in LLM training workloads.*

We further apply a first-order analytic model to GPT-175B, as depicted in Fig. 15, where C_{comp} , C_{recomp} , C_{access} and C_{comm} denotes the computation load, recomputation load, DRAM access and communication load, respectively. η represents the computation load associated with each byte of data. As can be seen, this model fails to capture the aforementioned insights and consistently favors configs with the largest DRAM capacity. This is essentially because the knapsack-like problem solved by WATOS is NP-hard and typically requires either complex multi-dimensional dynamic programming [78, 81] or heuristic algorithms [12, 34, 75]. This again confirms the necessity of using WATOS for exploring wafer-scale architectures under realistic training conditions.

C. Overall Performance

We compare the optimal WSC configuration (Config 3) with the Megatron-LM [122], a SOTA GPU-based LLM training system, referred to as MG-GPU. To ensure a fair comparison, the Megatron setup consists of 8×Blackwell Ultra 288GB GPUs, connected via 1.8 TB/s intra-node bandwidth. In terms of compute resources, MG-GPU offers a total of 40,000 TFLOPS, slightly exceeding the 39,648 TFLOPS provided by the WSC. To ensure fairness, MG-GPU’s DRAM is scaled from 2304 GB to 3920 GB to match the WSC, while both systems maintain equal DRAM bandwidth of 2 TB/s. Also, we directly apply Megatron’s scheduling strategy and Cerebras weight streaming strategy to the WSC, denoted as MG-wafer and Cerebras, respectively. For MG-wafer, we determine TP and PP sizes using Megatron, enumerate all feasible physical shapes on wsc (e.g., 1×4, 2×2, 4×1 for TP=4), place them in the naive serpentine arrangement (Fig. 11(a)) and evaluate the performance. We pick the best config as results for MG-wafer.

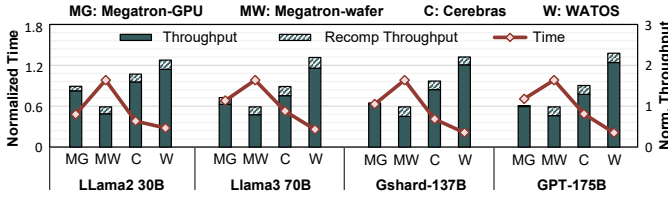


Fig. 16. Overall performance comparisons among Megatron-GPU, Megatron-wafer, Cerebras and WATOS.

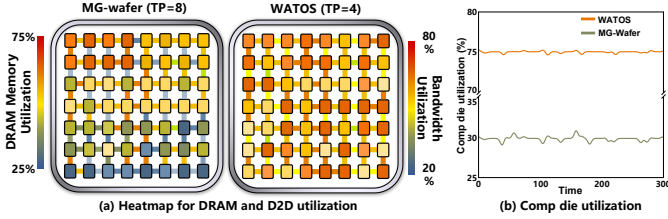


Fig. 17. DRAM memory, D2D and computation utilization comparisons between MG-wafer and WATOS for GPT 175B.

Fig. 16 compares the normalized throughput and training time across various LLM models. Compared to MG-GPU, WATOS achieves a $1.92\times$ higher throughput and $1.75\times$ shorter iteration time. Against MG-wafer and Cerebras, WATOS achieves up to $2.74\times$ and $1.53\times$ higher throughput, along with $2.45\times$ and $1.31\times$ shorter iteration time, respectively. Despite fewer compute resources, WATOS outperforms due to efficient operator execution and training-aware scheduling tailored to wafer-scale architectures. The performance gap between MG-wafer and MG-GPU stems from a 23% reduction in memory resources on MG-wafer and Megatron’s scheduling policy is optimized for GPU clusters, lacking the hardware-aware refinements required for wafer-scale systems. Notably, the proportion of recomputation in WATOS is only 30% to 60% of that in MG-Wafer, exhibiting the effectiveness of the proposed memory-balancing scheduling to reduce pipeline bubbles caused by recomputation and promote training efficiency. Compared to Cerebras, the iteration time reduction mainly stems from lower communication overhead and becomes more pronounced under small batch sizes and short sequences, up to a 187.4% improvement, because the communication cost of weight streaming scales proportionally with model parallelism degree. These results underscore the effectiveness of WATOS on WSCs for efficient LLM training.

Resource Utilization. Fig. 17 presents the heatmap under GPT-175B. As shown, WATOS with TP=4 achieves higher DRAM utilization and bandwidth efficiency than MG-wafer with TP=8. This is because MG-wafer suffers from inefficient resource partitioning and placement, leading to longer communication paths and frequent congestion that stalls computation. As a result, the compute die utilization in MG-wafer is only about 40% of that in WATOS. This highlights an insight: *With efficient resource allocation and memory scheduling strategies, small tensor parallelism can exhibit better performance on WSCs.*

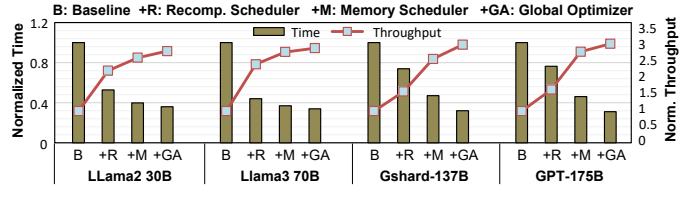


Fig. 18. Ablation performance of the WATOS.

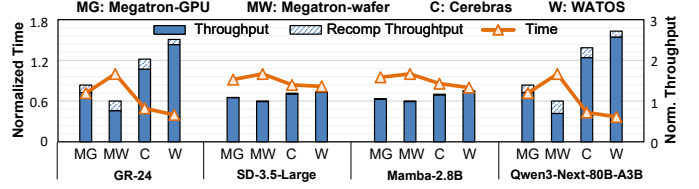


Fig. 19. WATOS’s performance on different emerging models.

D. Ablation Experiments

To assess the impact of WATOS optimizations, we conduct an ablation study on the 56-die wafer (Config 3). The baseline uses naive parallelism with fixed TP=8 and PP=7, without WATOS’s enhancements. Optimizations are then incrementally applied: **+R** enables GCMR recomputation scheduler, **+M** adds a location-aware memory scheduler, **+GA** incorporates the GA-based global optimizer.

As depicted in Fig. 18, we make the following observations: (1) As the model size increases, the performance benefit of the centralized scheduler diminishes. (2) In contrast, the performance gains from the memory-aware scheduler and recomputation grow with larger models. This is because smaller models typically require fewer pipeline stages, resulting in relatively mild memory imbalance issues and thus limited opportunities for memory scheduling optimization. In contrast, as model size increases, the pipeline depth grows, making memory scheduling critical for maintaining computational efficiency. Moreover, larger models are more susceptible to memory overflow, which amplifies the benefits of recomputation-based scheduling. These results highlight that the coordinated use of memory-aware, and recomputation schedulers in WATOS enables efficient training across diverse LLM scales.

VI. DISCUSSION

A. DSE Methods Analysis

Fig. 20 compares the performance of seven representative DSE studies for training LLMs under the WSC setting. We reproduce these works and capture their performance on WSC, including the DNN accelerator DSE framework Timeloop [105], the training-aware optimization DFModel [59], Calculon [47], two chiplet-based DSE frameworks: Hecton [46], Gemini [5], and two wafer-scale DSE schemes: PD [158], WSC-LLM [156]. Five key insights are made: 1) Timeloop performs worst as it targets only core-level workload partitioning, neglecting DRAM-aware and inter-die optimizations. 2) DFModel and Calculon partially improve performance by considering multi-dimensional parallel spaces. Calculon’s additional use of training memory-saving techniques provides

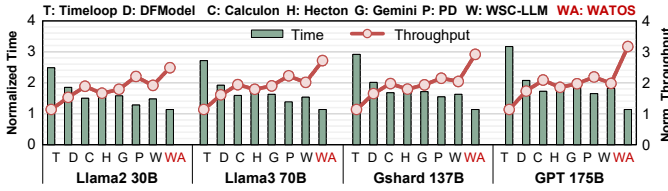


Fig. 20. Performance comparisons among WATOS and DSE methods.

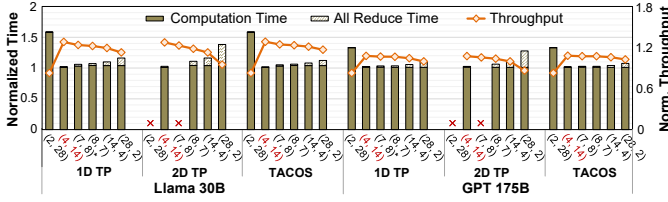


Fig. 21. Performance of different TP strategies and (TP, PP) configs.

more performance gains. **3)** Hecaton and Gemini fully account for communication in a 2D mesh, but as chiplet-oriented designs, they focus on reducing DRAM accesses rather than DRAM capacity, which leads to suboptimal performance. Moreover, Hecaton’s 2D TP relies on bypass links, resulting in additional communication costs on a 2D mesh topology. **4)** PD explores optimal topologies and logical designs in topological spaces but does not alleviate DRAM scarcity on WSCs, and its interconnect-focused design can worsen memory constraints. **5)** WSC-LLM explores the optimal LLM inference architecture under area constraints; however, its design space is sub-optimal due to the lack of recomputation-aware optimization. **Overall**, WATOS achieves superior performance by jointly considering WSC topology constraints, area trade-offs, and memory balance.

B. Expansion of Parallelism Search Space

Fig. 21 demonstrates WATOS’s performance in the expanded parallelism search space, including 2D TP proposed by GSPMD [155], RingBiOdd [62] and TACOS [151]. The WSC configuration remains consistent with Config3. Notably, RingBiOdd is employed to implement 7-instance TP that cannot be handled by the naive AllReduce [11].

Fig. 21 illustrates two key insights: **1)** The expanded parallel search space does not alter the optimal design point. Although TACOS and RingBiOdd support odd TP instances and TACOS outperforms at larger TP sizes, they still cannot overcome the increasing communication overhead as TP size grows. **2)** 2D TP yields the worst performance on the 2D mesh topology. While 2D TP can decompose large TPs, it is not tailored for LLMs, leading to higher communication volume and significant tail latency on a 2D mesh. Collectively, 2D TP, RingBiOdd, and TACOS expand WATOS’s parallel search space while leaving the optimal design point unchanged.

C. Architectural Generality

Fig. 19 demonstrates remarkable generality of WATOS across emerging models, including Generative Recommender [162] for recommendation, Stable Diffusion [20] for image

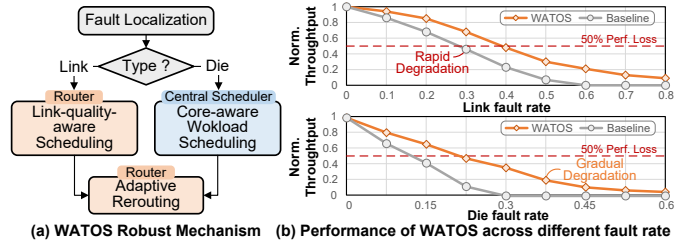


Fig. 22. The robustness and reliability design of WATOS.

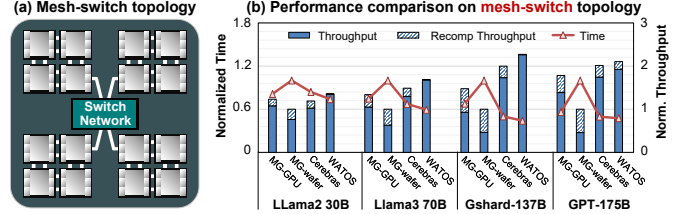


Fig. 23. WATOS performance on Mesh-switch topology.

and video generation, as well as new LLM architectures such as Mamba [14, 27] and Qwen3-Next [111], which are based on state space models and linear gated attention, respectively. The hardware configuration remains consistent with Config 3.

The strong generality of WATOS stems from three key factors. **1)** WATOS offers configurable architectural parameters to enable adaptation to diverse wafer-scale hardware setups and performs end-to-end scheduling to optimize large-scale model training. **2)** WATOS is operator-centric rather than model-specific, allowing it to accommodate new model workloads by extending DNN predictor, TP engine and compute die configurations without hardware modifications whenever new operators emerge. **3)** WATOS targets structural characteristics common to large-scale neural network training, addressing memory imbalance across pipeline stages and employing adaptive recomputation strategies rather than relying on any specific LLM or hardware architecture. Overall, WATOS demonstrates strong generality in large-scale model training rather than being a niche framework tailored for a niche architecture.

D. Robustness and reliability

As shown in Fig. 22 (a), WATOS introduces a 3-stage system-level robustness design: **1)** fault localization and classification, **2)** link-quality- and core-aware workload scheduling, and **3)** adaptive rerouting. **For link faults**, the router continuously monitors the quality of its connected links, such as packet loss rate and peak D2D bandwidth. Upon detecting degradation, it proactively reduces the communication load on the affected links and reroutes the excess traffic to the nearest alternative path using well-established routing algorithms [92, 109]. In the rare case of a complete link failure, no traffic is allocated to the broken link. **For die faults**, prolonged operation may lead to core degradation, resulting in reduced die performance. The central scheduler dynamically adjusts

workload distribution based on the degree of degradation, assigning less workload to the faulty die and redistributing tasks to healthy ones to maintain computation balance. Die failures, rare but critical, trigger the WATOS to mark the faulty die and its links as unavailable, excluding them from further workload allocation.

To evaluate fault-tolerance performance, we conduct experiments on WSC Config 3 across diverse LLM workloads, using the non-robust version of WATOS as the baseline and manually injecting failures. As depicted in Fig. 22, under a 20% link fault rate and a 20% die fault rate, the fault-tolerant WATOS achieves 18% and 35% higher throughput, respectively, benefiting from the system-level robustness optimization.

E. Topology Compatibility

Fig. 23 evaluates the performance of WATOS on mesh-switch topology proposed by [158]. As illustrated in Fig. 23 (a), we reconfigure Config3 to 48 dies arranged in a 12×2×2 mesh with a switch network offering 1.6 TB/s of bandwidth. The GPU baseline is scaled to ensure equivalent compute capability. Fig. 23 (b) illustrates that WATOS maintains superior performance compared to Megatron and Cerebras on the Mesh-switch topology, because: **1)** WATOS restricts TP within the mesh to fully leverage its high bandwidth and routes the lightweight inter-stage communication via the switch; **2)** the flexible switch enhances communication within mem_pair, alleviating potential congestion. By contrast, Megatron’s lack of mesh awareness leads to oversized TP and switch-limited All-Reduce, while Cerebras’ weight streaming similarly underutilizes mesh bandwidth and remains switch-bound. In such case, WATOS sustains high performance on mesh-switch topologies, demonstrating strong compatibility across diverse interconnect topologies.

3D Stacking variants. The 3D stacking [68, 69, 164] which vertically places DRAM on top of compute dies fundamentally shifts the memory access pattern and architectural trade-offs on WSC: **1)** DRAM access exhibits a local-remote gap. Local DRAM accesses traverse only the hybrid bonding interface, whereas remote accesses to DRAM on other compute dies must go through the NoC. **2)** 3D stacking decouples area competition between DRAM and compute dies, which allows fully allocating IOs to D2D interconnects, enabling larger DRAM capacity, higher compute density and increased D2D bandwidth across the wafer. Nonetheless, 3D stacking does not fundamentally alter the intrinsic characteristics of LLM training on WSCs: **1)** Communication relies on a high-bandwidth 2D mesh, which achieves high utilization for small TP size. **2)** Memory imbalance across pipeline stages necessitates recomputation. **3)** Unbalanced recomputation introduces bubbles, degrading performance. Thus, WATOS still remains competitive under 3D stacking, with a more relaxed trade-off.

F. Scalability for Multi-WSC Scenarios

We construct a WSC node composed of four Config-3 wafers and compare its performance against Megatron [122] to evaluate the scalability of WATOS, which comprises four

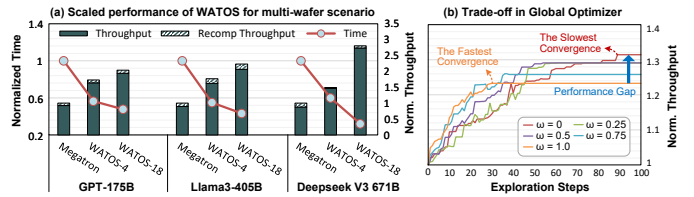


Fig. 24. (a) WATOS performance on multi-wafer scenarios. (b) Time-performance trade-off in the global optimizer.

nodes, each containing eight NVIDIA Blackwell ultra GPUs. For wafer-to-wafer (W2W) interconnect bandwidth, we consider two configurations: 1) WATOS-18, which employs a SOTA W2W interconnect [127] delivering 1.8 TB/s bandwidth; and 2) WATOS-4, which adopts a 400 GB/s W2W bandwidth configuration, equivalent to the inter-node bandwidth of Megatron. Further, we evaluate the capability of WATOS in training ultra-large models, including LLaMA3-405B [84] and Deepseek V3-671B [17].

As shown in Fig. 24 (a), two key insights emerge: 1) WATOS consistently outperforms Megatron in both high- and low-bandwidth W2W configurations; 2) WATOS achieves greater performance gains when scaling to ultra-large LLMs, demonstrating superior scalability. These findings arise from two main factors. For insight (1), WATOS outperforms for its ability to fully utilize the compute and memory resources within a single wafer, thereby reducing the reliance on W2W communication. For Insight (2), the scalability advantage stems from the high memory demand of large models. For example, Llama3-405B requires around 5670 GB of memory to store model weights, optimizer states, and gradients. As a result, Megatron must distribute the model across at least three 8-GPU servers. In contrast, two WSCs are sufficient, requiring at most a hop cross-wafer communication. Therefore, even WATOS-4 can achieve significant performance gains.

Hardware DSE. With the proposed hardware template, we explore the design space at die granularity, considering dies from 200 mm² to 600 mm², categorized as Small (< 400 mm²) or Large, and as Square (aspect ratio < 1.2) or Rectangle. The DSE objective is the product of memory capacity and throughput. As depicted in Fig. 25, under diverse workloads, Small Square configurations deliver superior performance by providing longer edges for D2D links and better area utilization, whereas Rectangle layouts underutilize area along single dimension, reducing both throughput and memory capacity. However, the high power density of Small Square configurations imposes strict cooling and power delivery constraints, leading current WSCs to favor Large Square design.

VII. RELATED WORKS

LLM training framework. Numerous frameworks [29, 60, 71, 90, 112, 116, 122, 129, 167] have been developed to improve LLM training efficiency on GPUs. For example, Alpha [167] decomposes the parallelism space into inter- and intra-operator dimensions to generate optimized execution plans, while Colossal-AI [71] supports modular parallelism

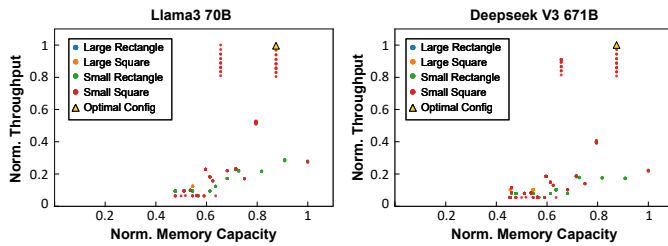


Fig. 25. Hardware DSE. Points of the same color denote configurations with the same die size category (Small or Large) and shape (Square or Rectangle), while different markers indicate different size categories and shape settings.

across data, tensor, and pipeline levels. However, these works are tailored to fully-connected GPUs and are not optimized for WSCs with 2D mesh interconnects. Thus, they overlook opportunities to exploit on-wafer bandwidth for fine-grained resource allocation.

Architectural DSE for Die-Level. Numerous studies [36, 37, 82, 105, 153, 160] have been devoted to architectural exploration. For example, Timeloop [105] develop a workload mapping-exploration framework to systematically optimize DNN accelerator designs. Sparseloop [153] extends sparse workloads, while Ruby [37] further handles imperfectly-factorized mappings. Regarding DSE methods, many works [2, 15, 26, 55, 118, 125, 148] employ genetic algorithms. Harpocrates [55] uses program mutation operators to automatically generate efficient test programs, while [125] proposes a variable-length encoding scheme with tailored operators to optimize CNN architectures. These operators are task-specific and difficult to generalize across training tasks on WSC.

For communication DSE. Several works [22, 47, 59, 62, 114, 115, 132, 151] explore the design space of parallelism and network topology. FRED [114] investigates the optimal switch topology and corresponding parallelization strategies at the wafer scale. TACOS [151] searches for optimal collective communication algorithms for a given topology by leveraging a time-expanded network representation and a link-chunk matching algorithm. Nonetheless, these approaches lack consideration of DRAM capacity during LLM training.

For chiplets. Current studies investigate architecture [5, 52, 99, 163, 165], dataflow [24, 98] and SRAM optimizations [25, 120]. However, these works focus on DNN inference in the chiplet scale, whereas our focus is on optimizing LLM training efficiency in WSCs. **For WSCs**, existing works [7, 23, 31, 40, 67, 101, 102, 114, 135, 144, 149, 156–158, 161, 169] have explored the design space of wafer-scale architectures, as well as floorplan design [50, 76, 80, 100]. However, existing works predominantly focus on inference, leaving training strategy co-design largely unexplored. While TMAC [144] pioneers the exploration of resource trade-offs under constrained wafer-scale area for recomputation, it lacks a global optimization strategy, which makes it difficult to identify the optimal design point. In summary, to the best of our knowledge, no prior work has systematically investigated

optimal parallelism strategies and resource allocation for LLM training on wafer-scale systems, making WATOS the first to address this problem.

VIII. CONCLUSION

This paper presents WATOS, an efficient framework for co-exploring LLM training and architecture on WSCs. Leveraging WSCs’ high D2D bandwidth and unique topology, WATOS optimizes parallelism, recomputation scheduling, placement, and memory allocation to improve LLM training performance. Experiments show that WATOS achieves $2.74\times$ throughput gains over Megatron and $1.53\times$ than Cerebras.

ACKNOWLEDGMENTS

This work was supported in part by the National Science and Technology Major Project under Grant 2022ZD0115200; the NSFC under Grant 62125403, and Grant 92164301; Beijing S&T Project Z221100007722023; in part by the project funding for the 2022 Special Project on Industrial Foundation Reconstruction and High Quality Development of Manufacturing Industry CEIEC-2022-ZM020245; in part by the Beijing National Research Center for Information Science and Technology; and in part by the Beijing Advanced Innovation Center for Integrated Circuits.

REFERENCES

- [1] A. A. Bajwa, S. Jangam, S. Pal, B. Vaisband, R. Irwin, M. Goorsky, and S. S. Iyer, “Demonstration of a heterogeneously integrated system-on-wafer (SoW) assembly,” in *2018 IEEE 68th Electronic Components and Technology Conference (ECTC)*. IEEE, 2018, pp. 1926–1930.
- [2] J. Bi, Q. Guo, X. Li, Y. Zhao, Y. Wen, Y. Guo, E. Zhou, X. Hu, Z. Du, and L. Li, “Heron: Automatically constrained high-performance library generation for deep learning accelerators,” in *Proceedings of the 28th ACM International Conference on Architectural Support for Programming Languages and Operating Systems, Volume 3*, 2023, pp. 314–328.
- [3] T. Brown, B. Mann, N. Ryder, M. Subbiah, J. D. Kaplan, P. Dhariwal, A. Neelakantan, P. Shyam, G. Sastry, and A. Askell, “Language models are few-shot learners,” *Advances in neural information processing systems*, vol. 33, pp. 1877–1901, 2020.
- [4] N. Burgess, J. Milanovic, N. Stephens, K. Monachopoulos, and D. Mansell, “Bfloat16 processing for neural networks,” in *2019 IEEE 26th Symposium on Computer Arithmetic (ARITH)*. IEEE, 2019, pp. 88–91.
- [5] J. Cai, Z. Wu, S. Peng, Y. Wei, Z. Tan, G. Shi, M. Gao, and K. Ma, “Gemini: Mapping and architecture co-exploration for large-scale DNN chiplet accelerators,” in *2024 IEEE International Symposium on High-Performance Computer Architecture (HPCA)*. IEEE, 2024, pp. 156–171.
- [6] Cerebras, “Cerebras systems: Achieving industry best AI performance through a

- systems approach,” 2021, [Online]. Available: <https://8968533.fs1.hubspotusercontent-na1.net/hubfs/8968533/Whitepapers/Cerebras-CS-2-Whitepaper.pdf>.
- [7] S. Chen, S. Pal, and R. Kumar, “Waferscale network switches,” in *Proceedings of the 50th Annual International Symposium on Computer Architecture*, 2021.
 - [8] T. Chen, B. Xu, C. Zhang, and C. Guestrin, “Training deep nets with sublinear memory cost,” *arXiv preprint arXiv:1604.06174*, 2016.
 - [9] T. Chen, Z. Du, N. Sun, J. Wang, C. Wu, Y. Chen, and O. Temam, “Diannao: A small-footprint high-throughput accelerator for ubiquitous machine-learning,” *ACM SIGARCH Computer Architecture News*, vol. 42, no. 1, pp. 269–284, 2014.
 - [10] Y.-H. Chen, T. Krishna, J. S. Emer, and V. Sze, “Eyeriss: An energy-efficient reconfigurable accelerator for deep convolutional neural networks,” *IEEE journal of solid-state circuits*, vol. 52, no. 1, pp. 127–138, 2016.
 - [11] Z. Chen, X. Liu, M. Li, Y. Hu, H. Mei, H. Xing, H. Wang, W. Shi, S. Liu, and Y. Xu, “Rina: Enhancing ring-allreduce with in-network aggregation in distributed model training,” in *2024 IEEE 32nd International Conference on Network Protocols (ICNP)*. IEEE, 2024, pp. 1–12.
 - [12] P. C. Chu and J. E. Beasley, “A genetic algorithm for the multidimensional knapsack problem,” *Journal of heuristics*, vol. 4, no. 1, pp. 63–86, 1998.
 - [13] T. Dao, “Flashattention-2: Faster attention with better parallelism and work partitioning,” *arXiv preprint arXiv:2307.08691*, 2023.
 - [14] T. Dao and A. Gu, “Transformers are SSMS: Generalized models and efficient algorithms through structured state space duality,” *arXiv preprint arXiv:2405.21060*, 2024.
 - [15] P. V. T. Dat, L. Doan, and H. T. T. Binh, “Hsevo: Elevating automatic heuristic design with diversity-driven harmony search and genetic algorithm using LLMs,” in *Proceedings of the AAAI Conference on Artificial Intelligence*, vol. 39, no. 25, 2025, pp. 26 931–26 938.
 - [16] J. Dean, G. Corrado, R. Monga, K. Chen, M. Devin, M. Mao, M. Ranzato, A. Senior, P. Tucker, and K. Yang, “Large scale distributed deep networks,” *Advances in neural information processing systems*, vol. 25, 2012.
 - [17] DeepSeek-AI, “Deepseek-v3 technical report,” 2025. [Online]. Available: <https://arxiv.org/abs/2412.19437>
 - [18] P. Dong, Y. Tan, X. Liu, P. Luo, Y. Liu, L. Liang, Y. Zhou, D. Pang, M.-T. Yung, D. Zhang, and F. Tu, “A 28nm 0.22 $\mu\text{J}/\text{token}$ memory-compute-intensity-aware CNN-Transformer accelerator with hybrid-attention-based layer-fusion and cascaded pruning for semantic-segmentation,” in *2025 IEEE International Solid-State Circuits Conference (ISSCC)*, vol. 68. IEEE, 2025, pp. 01–03.
 - [19] X. L. Dong, S. Moon, Y. E. Xu, K. Malik, and Z. Yu, “Towards next-generation intelligent assistants leveraging LLM techniques,” in *Proceedings of the 29th ACM SIGKDD Conference on Knowledge Discovery and Data Mining*, 2023, pp. 5792–5793.
 - [20] P. Esser, S. Kulal, A. Blattmann, R. Entezari, J. Müller, H. Saini, Y. Levi, D. Lorenz, A. Sauer, and F. Boesel, “Scaling rectified flow transformers for high-resolution image synthesis,” in *Forty-first international conference on machine learning*, 2024.
 - [21] S. Fan, Y. Rong, C. Meng, Z. Cao, S. Wang, Z. Zheng, C. Wu, G. Long, J. Yang, and L. Xia, “DAPPLE: A pipelined data parallel approach for training large models,” in *Proceedings of the 26th ACM SIGPLAN Symposium on Principles and Practice of Parallel Programming*, 2021, pp. 431–445.
 - [22] H. Farrokhbakht, P. V. Gratz, T. Krishna, J. San Miguel, and N. E. Jerger, “Stay in your lane: A NoC with low-overhead multi-packet bypassing,” in *2022 IEEE International Symposium on High-Performance Computer Architecture (HPCA)*. IEEE, 2022, pp. 957–970.
 - [23] Y. Feng and K. Ma, “Switch-less dragonfly on wafers: A scalable interconnection architecture based on wafer-scale integration,” *arXiv preprint arXiv:2407.10290*, 2024.
 - [24] M. Gao, X. Yang, J. Pu, M. Horowitz, and C. Kozyrakis, “Tangram: Optimized coarse-grained dataflow for scalable NN accelerators,” in *Proceedings of the 24th International Conference on Architectural Support for Programming Languages and Operating Systems*, 2019, pp. 807–820.
 - [25] R. Garg, H. Kwon, E. Qin, Y.-H. Chen, T. Krishna, and L. Lai, “Pipeorgan: Efficient inter-operation pipelining with flexible spatial organization and interconnects,” *arXiv preprint arXiv:2405.01736*, 2024.
 - [26] M. Giordano, R. Doshi, Q. Lu, and B. Murmann, “Tinyforge: A design space exploration to advance energy and silicon area trade-offs in tinyml compute architectures with custom latch arrays,” in *Proceedings of the 29th ACM International Conference on Architectural Support for Programming Languages and Operating Systems, Volume 3*, 2024, pp. 1033–1047.
 - [27] A. Gu and T. Dao, “Mamba: Linear-time sequence modeling with selective state spaces,” in *First Conference on Language Modeling*, 2024.
 - [28] H. Guo, S. Cao, L. Li, and X. Zhang, “A review on the mainstream through-silicon via etching methods,” *Materials Science in Semiconductor Processing*, vol. 137, p. 106182, 2022.
 - [29] D. Gurevin, M. Shan, S. Huang, M. A. Hasan, C. Ding, and O. Khan, “Prunegnn: Algorithm-architecture pruning framework for graph neural network acceleration,” in *2024 IEEE International Symposium on High-Performance Computer Architecture (HPCA)*. IEEE, 2024, pp. 108–123.
 - [30] Y. Han, H. Xu, M. Lu, H. Wang, J. Huang, Y. Wang, Y. Wang, F. Min, Q. Liu, M. Liu *et al.*, “The big chip: Challenge, model and architecture,” *Fundamental Research*, vol. 4, no. 6, pp. 1431–1441, 2024.

- [31] C. He, Y. Huang, P. Mu, Z. Miao, J. Xue, L. Ma, F. Yang, and L. Mai, "WaferLLM: Large language model inference at wafer scale," *arXiv preprint arXiv:2502.04563*, 2025.
- [32] X. He, J. Sun, H. Chen, and D. Li, "Campo: Cost-aware performance optimization for mixed-Precision neural network training," in *2022 USENIX Annual Technical Conference (USENIX ATC 22)*, 2022, pp. 505–518.
- [33] K. Hegde, P.-A. Tsai, S. Huang, V. Chandra, A. Parashar, and C. W. Fletcher, "Mind mappings: enabling efficient algorithm-accelerator mapping space search," in *Proceedings of the 26th ACM International Conference on Architectural Support for Programming Languages and Operating Systems*, 2021, pp. 943–958.
- [34] C. S. Hiremath, *New heuristic and metaheuristic approaches applied to the multiple-choice multidimensional knapsack problem*. Wright State University, 2008.
- [35] J. H. Holland, "Genetic algorithms," *Scientific american*, vol. 267, no. 1, pp. 66–73, 1992.
- [36] C. Hong, Q. Huang, G. Dinh, M. Subedar, and Y. S. Shao, "Dosa: Differentiable model-based one-loop search for DNN accelerators," in *Proceedings of the 56th Annual IEEE/ACM International Symposium on Microarchitecture*, 2023, pp. 209–224.
- [37] M. Horeni, P. Taheri, P.-A. Tsai, A. Parashar, J. Emer, and S. Joshi, "Ruby: Improving hardware efficiency for tensor algebra accelerators through imperfect factorization," in *2022 IEEE International Symposium on Performance Analysis of Systems and Software (ISPASS)*. IEEE, 2022, pp. 254–266.
- [38] S. Hou, C. H. Lee, T.-D. Wang, H. C. Hou, and H.-P. Hu, "Supercarrier redistribution layers to realize ultra large 2.5 D wafer scale packaging by CoWoS," in *2023 IEEE 73rd Electronic Components and Technology Conference (ECTC)*. IEEE, 2023, pp. 510–514.
- [39] C.-H. Hsia, S. Park, S. Watanabe, M. Arnold, Z. El-Mekki, M. Delande, E. Shafahian, P. K. Gowda, H. Struyf, and A. Radisic, "Wafer-level electrochemical deposition and processing of nanotwinned Cu RDL," in *2024 IEEE International Interconnect Technology Conference (IITC)*. IEEE, 2024, pp. 1–3.
- [40] Y. Hu, X. Lin, H. Wang, Z. He, X. Yu, J. Zhang, Q. Yang, Z. Xu, S. Guan, and J. Fang, "Wafer-scale computing: Advancements, challenges, and future perspectives," *IEEE Circuits and Systems Magazine*, vol. 24, no. 1, pp. 52–81, 2024.
- [41] Y.-C. Hu, Y.-M. Liang, H.-P. Hu, C.-Y. Tan, C.-T. Shen, C.-H. Lee, and S. Hou, "CoWoS architecture evolution for next generation HPC on 2.5D system in package," in *2023 IEEE 73rd Electronic Components and Technology Conference (ECTC)*. IEEE, 2023, pp. 1022–1026.
- [42] J. Huang, P. Majumder, S. Kim, A. Muzahid, K. H. Yum, and E. J. Kim, "Communication algorithm-architecture co-design for distributed deep learning," in *Proceedings of the 48th Annual International Symposium on Computer Architecture*. IEEE, 2021, p. 181–194.
- [43] J. Huang, H. Kim, N. Wang, J. Kang, H. Shah, E. K. Lee, M. Zhang, F. Lai, and N. S. Kim, "NetZIP: Algorithm/hardware co-design of in-network lossless compression for distributed large model training," in *Proceedings of the 58th IEEE/ACM International Symposium on Microarchitecture*, 2025, pp. 609–625.
- [44] P. Huang, C. Lu, W. Wei, C. Chiu, K. Ting, C. Hu, C. Tsai, S. Hou, W. Chiou, and C. Wang, "Wafer level system integration of the fifth generation CoWoS®-S with high performance Si interposer at 2500 mm²," in *2021 IEEE 71st Electronic Components and Technology Conference (ECTC)*. IEEE, 2021, pp. 101–104.
- [45] Y. Huang, Y. Cheng, A. Bapna, O. Firat, D. Chen, M. Chen, H. Lee, J. Ngiam, Q. V. Le, and Y. Wu, "Gpipe: Efficient training of giant neural networks using pipeline parallelism," *Advances in neural information processing systems*, vol. 32, 2019.
- [46] Z. Huang, S. Fan, C. Tang, X. Lin, S. Deng, and Y. Liu, "Hecaton: Training large language models with scalable chiplet systems," *arXiv preprint arXiv:2407.05784*, 2024.
- [47] M. Isaev, N. McDonald, L. Dennison, and R. Vuduc, "Calculon: a methodology and tool for high-level co-design of systems and large language models," in *Proceedings of the International Conference for High Performance Computing, Networking, Storage and Analysis*, 2023, pp. 1–14.
- [48] P. Jain, A. Jain, A. Nrusimha, A. Gholami, P. Abbeel, J. Gonzalez, K. Keutzer, and I. Stoica, "Checkmate: Breaking the memory wall with optimal tensor rematerialization," *Proceedings of Machine Learning and Systems*, vol. 2, pp. 497–511, 2020.
- [49] Z. Jia, J. Thomas, T. Warszawski, M. Gao, M. Zaharia, and A. Aiken, "Optimizing DNN computation with relaxed graph substitutions," *Proceedings of Machine Learning and Systems*, vol. 1, pp. 27–39, 2019.
- [50] B. Jiang, J. Chen, J. Liu, L. Liu, F. Wang, X. Zhang, and E. F. Young, "CU. POKer: Placing DNNs on WSE with optimal kernel sizing and efficient protocol optimization," *IEEE Transactions on Computer-Aided Design of Integrated Circuits and Systems*, vol. 41, no. 6, pp. 1888–1901, 2021.
- [51] B. Jiao, J. Qiao, S. Jia, R. Liu, X. Wei, S. Yun, Y. Kong, Y. Ye, X. Du, and L. Yu, "Low stress TSV arrays for high-density interconnection," *Engineering*, vol. 38, pp. 201–208, 2024.
- [52] D. Kadiyala, S. Rashidi, T. Heo, A. Bambhaniya, T. Krishna, and A. Daglis, "Leveraging memory expansion to accelerate large-scale DL training," in *2024 IEEE International Symposium on Performance Analysis of Systems and Software (ISPASS)*. IEEE, 2024, pp. 292–294.
- [53] D. Kalamkar, D. Mudigere, N. Mellempudi, D. Das,

- K. Banerjee, S. Avancha, D. T. Vooturi, N. Jammalamadaka, J. Huang, and H. Yuen, "A study of BFLOAT16 for deep learning training," *arXiv preprint arXiv:1905.12322*, 2019.
- [54] S.-C. Kao, G. Jeong, and T. Krishna, "Confucius: Autonomous hardware resource assignment for dnn accelerators using reinforcement learning," in *2020 53rd Annual IEEE/ACM International Symposium on Microarchitecture (MICRO)*. IEEE, 2020, pp. 622–636.
- [55] N. Karystinos, O. Chatzopoulos, G.-M. Fragakoulis, G. Papadimitriou, D. Gizopoulos, and S. Gurumurthi, "Harpocrates: Breaking the silence of cpu faults through hardware-in-the-loop program generation," in *2024 ACM/IEEE 51st Annual International Symposium on Computer Architecture (ISCA)*. IEEE, 2024, pp. 516–531.
- [56] S. Kim, J. Lee, and H.-J. Yoo, "Slim-Llama: A 4.69 mW large-language-model processor with binary/ternary weights for billion-parameter Llama model," in *2025 IEEE International Solid-State Circuits Conference (ISSCC)*, vol. 68. IEEE, 2025, pp. 421–423.
- [57] T. Kim, H. Kim, G.-I. Yu, and B.-G. Chun, "Bpipe: Memory-balanced pipeline parallelism for training large language models," in *International Conference on Machine Learning*. PMLR, 2023, pp. 16 639–16 653.
- [58] T. Kim, Y. Wang, V. Chaturvedi, L. Gupta, S. Kim, Y. Kwon, and S. Ha, "Llmem: Estimating GPU memory usage for fine-tuning pre-trained LLMs," *arXiv preprint arXiv:2404.10933*, 2024.
- [59] S. Ko, N. Zhang, O. Hsu, A. Pedram, and K. Olukotun, "Dfmodel: Design space optimization of large-scale systems exploiting dataflow mappings," *arXiv preprint arXiv:2412.16432*, 2024.
- [60] V. A. Korthikanti, J. Casper, S. Lym, L. McAfee, M. Andersch, M. Shoeybi, and B. Catanzaro, "Reducing activation recomputation in large Transformer models," *Proceedings of Machine Learning and Systems*, vol. 5, pp. 341–353, 2023.
- [61] H. Kwon, P. Chatarasi, M. Pellauer, A. Parashar, V. Sarkar, and T. Krishna, "Understanding reuse, performance, and hardware cost of DNN dataflow: A data-centric approach," in *Proceedings of the 52nd Annual IEEE/ACM International Symposium on Microarchitecture*, 2019, pp. 754–768.
- [62] S. Laskar, P. Majhi, S. Kim, F. Mahmud, A. Muzahid, and E. J. Kim, "Enhancing collective communication in mcm accelerators for deep learning training," in *2024 IEEE International Symposium on High-Performance Computer Architecture (HPCA)*. IEEE, 2024, pp. 1–16.
- [63] J. H. Lau, "Recent advances and trends in multiple system and heterogeneous integration with TSV interposers," *IEEE Transactions on Components, Packaging and Manufacturing Technology*, vol. 13, no. 1, pp. 3–25, 2023.
- [64] J. H. Lau, G. C.-F. Chen, J. Y.-C. Huang, R. T.-S. Chou, C. C.-L. Yang, H.-N. Liu, and T.-J. Tseng, "Hybrid substrate by fan-out RDL-first panel-level packaging," *IEEE Transactions on Components, Packaging and Manufacturing Technology*, vol. 11, no. 8, pp. 1301–1309, 2021.
- [65] J. H. Lau, C.-T. Ko, K.-M. Yang, C.-Y. Peng, T. Xia, P. B. Lin, J. Chen, P. P.-C. Huang, H.-N. Liu, and T.-J. Tseng, "Panel-level fan-out RDL-first packaging for heterogeneous integration," *IEEE Transactions on Components, Packaging and Manufacturing Technology*, vol. 10, no. 7, pp. 1125–1137, 2020.
- [66] D. Lepikhin, H. Lee, Y. Xu, D. Chen, O. Firat, Y. Huang, M. Krikun, N. Shazeer, and Z. Chen, "Gshard: Scaling giant models with conditional computation and automatic sharding," *arXiv preprint arXiv:2006.16668*, 2020.
- [67] C.-r. LI, J.-h. FANG, S.-y. YIN, S.-j. WEI, and Y. HU, "Research on wafer-scale chip mapping task based on genetic algorithm," *Computer Engineering & Science*, vol. 46, no. 06, p. 993, 2024.
- [68] C. Li, Y. Yin, X. Wu, J. Zhu, Z. Gao, D. Niu, Q. Wu, X. Si, Y. Xie, and C. Zhang, "H2-LLM: Hardware-dataflow co-exploration for heterogeneous hybrid-bonding-based low-batch LLM inference," in *Proceedings of the 52nd Annual International Symposium on Computer Architecture*, 2025, pp. 194–210.
- [69] G. Li, R. Xu, R. Xu, Y. Qiu, R. Tuerhong, M. Zhang, L. Ye, and Y. Ma, "3D-SubG: A 3D stacked hybrid processing near/in-memory accelerator for subgraph GNNs," in *2025 62nd ACM/IEEE Design Automation Conference (DAC)*. IEEE, 2025, pp. 1–7.
- [70] J. Li, J. Xu, S. Huang, Y. Chen, W. Li, J. Liu, Y. Lian, J. Pan, L. Ding, H. Zhou *et al.*, "Large language model inference acceleration: A comprehensive hardware perspective," *arXiv preprint arXiv:2410.04466*, 2024.
- [71] S. Li, H. Liu, Z. Bian, J. Fang, H. Huang, Y. Liu, B. Wang, and Y. You, "Colossal-AI: A unified deep learning system for large-scale parallel training," in *Proceedings of the 52nd International Conference on Parallel Processing*, 2023, pp. 766–775.
- [72] S. Li and T. Hoefler, "Chimera: Efficiently training large-scale neural networks with bidirectional pipelines," in *Proceedings of the International Conference for High Performance Computing, Networking, Storage and Analysis*, 2021, pp. 1–14.
- [73] S. Lie, "Cerebras architecture deep dive: First look inside the hw/sw co-design for deep learning: Cerebras systems," in *2022 IEEE Hot Chips 34 Symposium (HCS)*. IEEE Computer Society, 2022, pp. 1–34.
- [74] S. Lie, "Inside the cerebras wafer-scale cluster," *IEEE Micro*, vol. 44, no. 3, pp. 49–57, 2024.
- [75] F.-T. Lin, C.-Y. Kao, and C.-C. Hsu, "Applying the genetic approach to simulated annealing in solving some NP-hard problems," *IEEE Transactions on systems, man, and cybernetics*, vol. 23, no. 6, pp. 1752–1767, 1993.
- [76] J. Liu, X. Zhang, S. Lin, X. Zang, J. Chen, B. Jiang,

- M. D. Wong, and E. F. Young, "Partition and place finite element model on wafer-scale engine," in *Proceedings of the 59th ACM/IEEE Design Automation Conference*, 2022, pp. 631–636.
- [77] Z. Liu, S. Cheng, H. Zhou, and Y. You, "Hanayo: Harnessing wave-like pipeline parallelism for enhanced large model training efficiency," in *Proceedings of the International Conference for High Performance Computing, Networking, Storage and Analysis*, 2023, pp. 1–13.
- [78] A. Lodi, S. Martello, and D. Vigo, "Approximation algorithms for the oriented two-dimensional bin packing problem," *European Journal of Operational Research*, vol. 112, no. 1, pp. 158–166, 1999.
- [79] H. Ltaief, Y. Hong, L. Wilson, M. Jacquelin, M. Ravasi, and D. E. Keyes, "Scaling the "memory wall" for multi-dimensional seismic processing with algebraic compression on Cerebras CS-2 systems," in *Proceedings of the International Conference for High Performance Computing, Networking, Storage and Analysis*, 2023, pp. 1–12.
- [80] C. Luo, Z. Su, and Z. Lü, "MS-CLS: An effective partitioning and placement metaheuristic for wafer-scale physics modeling," *IEEE Transactions on Emerging Topics in Computational Intelligence*, 2023.
- [81] S. Martello and P. Toth, *Knapsack problems: Algorithms and computer implementations*. John Wiley & Sons, Inc., 1990.
- [82] L. Mei, K. Goetschalckx, A. Symons, and M. Verhelst, "Defines: Enabling fast exploration of the depth-first scheduling space for DNN accelerators through analytical modeling," in *2023 IEEE International Symposium on High-Performance Computer Architecture (HPCA)*. IEEE, 2023, pp. 570–583.
- [83] Meta AI, "Llama 3 model card," 2024, [Online]. Available: https://github.com/meta-llama/llama3/blob/main/MODEL_CARD.md.
- [84] Meta AI, "Llama-3.1-405B," 2024, [Online]. Available: <https://huggingface.co/meta-llama/Llama-3.1-405B>.
- [85] P. Micikevicius, S. Narang, J. Alben, G. Diamos, E. Elsen, D. Garcia, B. Ginsburg, M. Houston, O. Kuchaiev, and G. Venkatesh, "Mixed precision training," *arXiv preprint arXiv:1710.03740*, 2017.
- [86] S. Moon, M. Li, G. K. Chen, P. C. Knag, R. K. Krishnamurthy, and M. Seok, "T-REX: A 68-to-567 μ s/token 0.41-to-3.95 μ J/token transformer accelerator with reduced external memory access and enhanced hardware utilization in 16nm FinFET," in *2025 IEEE International Solid-State Circuits Conference (ISSCC)*, vol. 68. IEEE, 2025, pp. 406–408.
- [87] G. E. Moore, "Cramming more components onto integrated circuits," *Proceedings of the IEEE*, vol. 86, no. 1, pp. 82–85, 1998.
- [88] S. Naffziger, K. Lepak, M. Paraschou, and M. Subramony, "AMD chiplet architecture for high-performance server and desktop products," in *2020 IEEE International Solid-State Circuits Conference-(ISSCC)*. IEEE, 2020, pp. 44–45.
- [89] D. Narayanan, A. Phanishayee, K. Shi, X. Chen, and M. Zaharia, "Memory-efficient pipeline-parallel DNN training," in *International Conference on Machine Learning*. PMLR, 2021, pp. 7937–7947.
- [90] D. Narayanan, M. Shoeybi, J. Casper, P. LeGresley, M. Patwary, V. Korthikanti, D. Vainbrand, P. Kashinkunti, J. Bernauer, and B. Catanzaro, "Efficient large-scale language model training on GPU clusters using Megatron-LM," in *Proceedings of the international conference for high performance computing, networking, storage and analysis*, 2021, pp. 1–15.
- [91] D. Nguyen, W. Yang, R. Anand, Y. Yang, and B. Mirza-soleiman, "Memory-efficient training of LLMs with larger mini-batches," *arXiv e-prints*, pp. arXiv-2407, 2024.
- [92] R. Niranjana Mysore, A. Pamboris, N. Farrington, N. Huang, P. Miri, S. Radhakrishnan, V. Subramanya, and A. Vahdat, "Portland: A scalable fault-tolerant layer 2 data center network fabric," in *Proceedings of the ACM SIGCOMM 2009 conference on Data communication*, 2009, pp. 39–50.
- [93] NVIDIA, "NVIDIA H100," 2022, [Online]. Available: <https://www.nvidia.com/en-us/data-center/h100>.
- [94] NVIDIA, "Megatron-LM," 2025, [Online]. Available: <https://github.com/NVIDIA/Megatron-LM>.
- [95] NVIDIA, "NVIDIA GB300," 2025, [Online]. Available: <https://www.nvidia.com/en-us/data-center/gb300-nv172/>.
- [96] NVIDIA, "NVIDIA GB200 NVL72: Powering the new era of computing," n.d., [Online]. Available: <https://www.nvidia.com/en-us/data-center/gb200-nv172/>.
- [97] NVIDIA Corporation, "NVIDIA DGX GH200: The next-generation AI supercomputer for the generative AI era," NVIDIA, Tech. Rep., 2023. [Online]. Available: <https://www.zhaocs.info/wp-content/uploads/2024/04/dgx-gh200-whitepaper.pdf>
- [98] M. Orenes-Vera, E. Tureci, M. Martonosi, and D. Wentzlaff, "DCRA: A distributed chiplet-based reconfigurable architecture for irregular applications," *arXiv preprint arXiv:2311.15443*, 2023.
- [99] M. Orenes-Vera, E. Tureci, M. Martonosi, and D. Wentzlaff, "Muchisim: A simulation framework for design exploration of multi-chip manycore systems," in *2024 IEEE International Symposium on Performance Analysis of Systems and Software (ISPASS)*. IEEE, 2024, pp. 48–60.
- [100] S. Özdemir, M. Khasawneh, S. Rao, and P. H. Madden, "Kernel mapping techniques for deep learning neural network accelerators," in *Proceedings of the 2022 International Symposium on Physical Design*, 2022, pp. 21–28.
- [101] S. Pal, *Scale-out packageless processing*. University of California, Los Angeles, 2021.
- [102] S. Pal, J. Liu, I. Alam, N. Cebry, H. Suhail, S. Bu, S. S.

- Iyer, S. Pamarti, R. Kumar, and P. Gupta, "Designing a 2048-chiplet, 14336-core waferscale processor," in *2021 58th ACM/IEEE Design Automation Conference (DAC)*. IEEE, 2021, pp. 1183–1188.
- [103] S. Pal, D. Petrisko, M. Tomei, P. Gupta, S. S. Iyer, and R. Kumar, "Architecting waferscale processors-A GPU case study," in *2019 IEEE International Symposium on High Performance Computer Architecture (HPCA)*. IEEE, 2019, pp. 250–263.
- [104] K. PANNER SELVAM and M. H. BRORSSON, "Can semi-supervised learning improve prediction of deep learning model resource consumption?" *International Journal of Advanced Computer Science and Applications*, vol. 15, no. 6, 2024.
- [105] A. Parashar, P. Raina, Y. S. Shao, Y.-H. Chen, V. A. Ying, A. Mukkara, R. Venkatesan, B. Khailany, S. W. Keckler, and J. Emer, "Timeloop: A systematic approach to dnn accelerator evaluation," in *2019 IEEE international symposium on performance analysis of systems and software (ISPASS)*. IEEE, 2019, pp. 304–315.
- [106] J. Park, S. Jang, O. Kwon, Y. Lee, and S. Hong, "Leveraging chiplet-locality for efficient memory mapping in multi-chip module GPUs," in *Proceedings of the 58th IEEE/ACM International Symposium on Microarchitecture*, 2025, pp. 1040–1057.
- [107] S. G. Patil, P. Jain, P. Dutta, I. Stoica, and J. Gonzalez, "Poet: Training neural networks on tiny devices with integrated rematerialization and paging," in *International Conference on Machine Learning*. PMLR, 2022, pp. 17 573–17 583.
- [108] A. Petrowski, G. Dreyfus, and C. Girault, "Performance analysis of a pipelined backpropagation parallel algorithm," *IEEE Transactions on Neural Networks*, vol. 4, no. 6, pp. 970–981, 1993.
- [109] Y.-A. Pignolet, S. Schmid, and G. Tredan, "Load-optimal local fast rerouting for resilient networks," in *2017 47th Annual IEEE/IFIP International Conference on Dependable Systems and Networks (DSN)*. IEEE, 2017, pp. 345–356.
- [110] B. Pudipeddi, M. Mesmakhosroshahi, J. Xi, and S. Bharadwaj, "Training large neural networks with constant memory using a new execution algorithm," *arXiv preprint arXiv:2002.05645*, 2020.
- [111] Qwen, "Qwen3-Next-80B-A3B-Instruct," 2025, [Online]. Available: <https://huggingface.co/Qwen/Qwen3-Next-80B-A3B-Instruct>.
- [112] S. Rajbhandari, J. Rasley, O. Ruwase, and Y. He, "Zero: Memory optimizations toward training trillion parameter models," in *SC20: International Conference for High Performance Computing, Networking, Storage and Analysis*. IEEE, 2020, pp. 1–16.
- [113] S. Rajbhandari, O. Ruwase, J. Rasley, S. Smith, and Y. He, "Zero-infinity: Breaking the GPU memory wall for extreme scale deep learning," in *Proceedings of the international conference for high performance computing, networking, storage and analysis*, 2021, pp. 1–14.
- [114] S. Rashidi, W. Won, S. Srinivasan, P. Gupta, and T. Krishna, "FRED: Flexible reduction-distribution interconnect and communication implementation for wafer-scale distributed training of DNN models," *arXiv preprint arXiv:2406.19580*, 2024.
- [115] S. Rashidi, W. Won, S. Srinivasan, S. Sridharan, and T. Krishna, "Themis: A network bandwidth-aware collective scheduling policy for distributed training of DL models," in *Proceedings of the 49th Annual International Symposium on Computer Architecture*, 2022, pp. 581–596.
- [116] J. Rasley, S. Rajbhandari, O. Ruwase, and Y. He, "Deepspeed: System optimizations enable training deep learning models with over 100 billion parameters," in *Proceedings of the 26th ACM SIGKDD international conference on knowledge discovery & data mining*, 2020, pp. 3505–3506.
- [117] J. Ren, S. Rajbhandari, R. Y. Aminabadi, O. Ruwase, S. Yang, M. Zhang, D. Li, and Y. He, "Zero-offload: Democratizing billion-scale model training," in *2021 USENIX Annual Technical Conference (USENIX ATC 21)*, 2021, pp. 551–564.
- [118] J. Ren, D. Xu, S. Yang, J. Zhao, Z. Li, C. Navasca, C. Wang, H. Xu, and D. Li, "Enabling large dynamic neural network training with learning-based memory management," in *2024 IEEE International Symposium on High-Performance Computer Architecture (HPCA)*. IEEE, 2024, pp. 788–802.
- [119] L. M. Schmitt, "Theory of genetic algorithms," *Theoretical Computer Science*, vol. 259, no. 1-2, pp. 1–61, 2001.
- [120] Y. S. Shao, J. Clemons, R. Venkatesan, B. Zimmer, M. Fojtik, N. Jiang, B. Keller, A. Klinefelter, N. Pinckney, and P. Raina, "Simba: Scaling deep-learning inference with multi-chip-module-based architecture," in *Proceedings of the 52nd Annual IEEE/ACM International Symposium on Microarchitecture*, 2019, pp. 14–27.
- [121] P.-C. Shih, A.-J. Su, K.-H. Tam, T.-C. Huang, K. Chuang, and J. Yeh, "SoW-X: A novel system-on-wafer technology for next generation AI server application," in *2025 IEEE 75th Electronic Components and Technology Conference (ECTC)*. IEEE, 2025, pp. 1–6.
- [122] M. Shoeybi, M. Patwary, R. Puri, P. LeGresley, J. Casper, and B. Catanzaro, "Megatron-LM: Training multi-billion parameter language models using model parallelism," *arXiv preprint arXiv:1909.08053*, 2019.
- [123] M. Song, K. Zhong, J. Zhang, Y. Hu, D. Liu, W. Zhang, J. Wang, and T. Li, "In-situ AI: Towards autonomous and incremental deep learning for IoT systems," in *2018 IEEE International Symposium on High Performance Computer Architecture (HPCA)*. IEEE, 2018, pp. 92–103.
- [124] M. Špet'ko, O. Vysocký, B. Jansík, and L. Říha, "DGX-A100 face to face DGX-2—performance, power and

- thermal behavior evaluation,” *Energies*, vol. 14, no. 2, p. 376, 2021.
- [125] Y. Sun, B. Xue, M. Zhang, G. G. Yen, and J. Lv, “Automatically designing CNN architectures using the genetic algorithm for image classification,” *IEEE transactions on cybernetics*, vol. 50, no. 9, pp. 3840–3854, 2020.
- [126] Z. Sun, H. Cao, Y. Wang, G. Feng, S. Chen, H. Wang, and W. Chen, “Adapipe: Optimizing pipeline parallelism with adaptive recomputation and partitioning,” in *Proceedings of the 29th ACM International Conference on Architectural Support for Programming Languages and Operating Systems, Volume 3*, 2024, pp. 86–100.
- [127] E. Talpes, D. Williams, and D. D. Sarma, “Dojo: The microarchitecture of Tesla’s exa-scale computer,” in *2022 IEEE Hot Chips 34 Symposium (HCS)*. IEEE Computer Society, 2022, pp. 1–28.
- [128] Z. Tan, H. Cai, R. Dong, and K. Ma, “NN-baton: DNN workload orchestration and chiplet granularity exploration for multichip accelerators,” in *2021 ACM/IEEE 48th Annual International Symposium on Computer Architecture (ISCA)*. IEEE, 2021, pp. 1013–1026.
- [129] H. Tang, S. Yang, Z. Liu, K. Hong, Z. Yu, X. Li, G. Dai, Y. Wang, and S. Han, “Torchsparse++: Efficient training and inference framework for sparse convolution on gpus,” in *Proceedings of the 56th Annual IEEE/ACM International Symposium on Microarchitecture*, 2023, pp. 225–239.
- [130] R. Thakur, R. Rabenseifner, and W. Gropp, “Optimization of collective communication operations in mpich,” *The International Journal of High Performance Computing Applications*, vol. 19, no. 1, pp. 49–66, 2005.
- [131] A. Tirumala and R. Wong, “Nvidia blackwell platform: Advancing generative AI and accelerated computing,” in *2024 IEEE Hot Chips 36 Symposium (HCS)*. IEEE Computer Society, 2024, pp. 1–33.
- [132] J. Tong, A. Itagi, P. Chatarasi, and T. Krishna, “Feather: A reconfigurable accelerator with data reordering support for low-cost on-chip dataflow switching,” in *2024 ACM/IEEE 51st Annual International Symposium on Computer Architecture (ISCA)*. IEEE, 2024, pp. 198–214.
- [133] H. Touvron, T. Lavril, G. Izacard, X. Martinet, M.-A. Lachaux, T. Lacroix, B. Rozière, N. Goyal, E. Hambro, and F. Azhar, “Llama: Open and efficient foundation language models,” *arXiv preprint arXiv:2302.13971*, 2023.
- [134] H. Touvron, L. Martin, K. Stone, P. Albert, A. Almahairi, Y. Babaei, N. Bashlykov, S. Batra, P. Bhargava, and S. Bhosale, “Llama 2: Open foundation and fine-tuned chat models,” *arXiv preprint arXiv:2307.09288*, 2023.
- [135] Z. Wan, Z. Cao, S. Li, P. Li, Q. Deng, W. Wang, K. Zhang, G. Liu, R. Zhang, and Q. Liu, “Architectural exploration for waferscale switching system,” *IEEE Transactions on Very Large Scale Integration (VLSI) Systems*, 2024.
- [136] H. Wang, B. Cheng, X. Tan, X. You, and C. Zhang, “An efficient approximate expectation propagation detector with block-diagonal Neumann-series,” *IEEE Transactions on Circuits and Systems I: Regular Papers*, vol. 70, no. 3, pp. 1403–1416, 2023.
- [137] H. Wang, J. Fang, X. Tang, Z. Yue, J. Li, Y. Qin, S. Guan, Q. Yang, Y. Wang, C. Li *et al.*, “SOFA: A compute-memory optimized sparsity accelerator via cross-stage coordinated tiling,” in *2024 57th IEEE/ACM International Symposium on Microarchitecture (MICRO)*. IEEE, 2024, pp. 1247–1263.
- [138] H. Wang, Y. Ji, Y. Shen, W. Song, M. Li, X. You, and C. Zhang, “An efficient detector for massive MIMO based on improved matrix partition,” *IEEE Transactions on Signal Processing*, vol. 69, pp. 2971–2986, 2021.
- [139] H. Wang, H. Wang, S. Wei, Y. Hu, and S. Yin, “Bit-stopper: An efficient transformer attention accelerator via stage-fusion and early termination,” *arXiv preprint arXiv:2512.06457*, 2025.
- [140] H. Wang, H. Wang, S. Wei, Y. Hu, and S. Yin, “Lapa: Log-domain prediction-driven dynamic sparsity accelerator for transformer model,” *arXiv preprint arXiv:2512.07855*, 2025.
- [141] H. Wang, H. Wang, Z. Yue, J. Liu, T. Wei, S. W. Y. Hu, and S. Yin, “BETA: A bit-Grained Transformer attention accelerator With efficient early termination,” *IEEE Transactions on Circuits and Systems II: Express Briefs*, 2025.
- [142] H. Wang, Z. Wang, Z. Yue, Y. Long, T. Wei, J. Yang, Y. Wang, C. Li, S. Wei, Y. Hu *et al.*, “MCBP: A memory-compute efficient LLM inference accelerator leveraging bit-slice-enabled sparsity and repetitiveness,” in *Proceedings of the 58th IEEE/ACM International Symposium on Microarchitecture*, 2025, pp. 1592–1608.
- [143] H. Wang, W. Xu, Z. Zhang, X. You, and C. Zhang, “An efficient stochastic convolution architecture based on fast FIR algorithm,” *IEEE Transactions on Circuits and Systems II: Express Briefs*, vol. 69, no. 3, pp. 984–988, 2021.
- [144] H. Wang, Q. Yang, T. Wei, X. Yu, C. Li, J. Fang, G. Lu, X. Dai, L. Liu, S. Jiang *et al.*, “TMAC: Training-targeted mapping and architecture co-exploration for wafer-scale chips,” *Integrated Circuits and Systems*, 2024.
- [145] H. Wang, Z. Zhang, X. You, and C. Zhang, “Low-complexity Winograd convolution architecture based on stochastic computing,” in *2018 IEEE 23rd International Conference on Digital Signal Processing (DSP)*. IEEE, 2018, pp. 1–5.
- [146] M. Wang, C.-c. Huang, and J. Li, “Supporting very large models using automatic dataflow graph partitioning,” in *Proceedings of the Fourteenth EuroSys Conference 2019*, 2019, pp. 1–17.
- [147] T. Wang, F. Feng, S. Xiang, Q. Li, and J. Xia, “Application defined on-chip networks for heterogeneous

- chipllets: An implementation perspective,” in *2022 IEEE International Symposium on High-Performance Computer Architecture (HPCA)*. IEEE, 2022, pp. 1198–1210.
- [148] Z. Wang, Y. Zhang, F. Wei, B. Wang, Y. Liu, Z. Hu, J. Zhang, X. Xu, J. He, and X. Wang, “Using analytical performance/power model and fine-grained DVFS to enhance AI accelerator energy efficiency,” in *Proceedings of the 30th ACM International Conference on Architectural Support for Programming Languages and Operating Systems*, vol. 1, 2025, pp. 1118–1132.
- [149] T. Wei, H. Wang, Z. Wang, S. Yin, and Y. Hu, “Spatial-aware orchestration of LLM attention on waferscale chips,” in *International Symposium on Advanced Parallel Processing Technologies*. Springer, 2025, pp. 386–391.
- [150] Wikichip, “Mask / Reticle,” 2022, [Online]. Available: <https://en.wikichip.org/wiki/mask>.
- [151] W. Won, M. Elavazhagan, S. Srinivasan, S. Gupta, and T. Krishna, “Tacos: Topology-aware collective algorithm synthesizer for distributed machine learning,” in *2024 57th IEEE/ACM International Symposium on Microarchitecture (MICRO)*. IEEE, 2024, pp. 856–870.
- [152] W. Won, T. Heo, S. Rashidi, S. Sridharan, S. Srinivasan, and T. Krishna, “Astra-sim2. 0: Modeling hierarchical networks and disaggregated systems for large-model training at scale,” in *2023 IEEE International Symposium on Performance Analysis of Systems and Software (ISPASS)*. IEEE, 2023, pp. 283–294.
- [153] Y. N. Wu, P.-A. Tsai, A. Parashar, V. Sze, and J. S. Emer, “Sparseloop: An analytical approach to sparse tensor accelerator modeling,” in *2022 55th IEEE/ACM International Symposium on Microarchitecture (MICRO)*. IEEE, 2022, pp. 1377–1395.
- [154] E. P. Xing, Q. Ho, W. Dai, J.-K. Kim, J. Wei, S. Lee, X. Zheng, P. Xie, A. Kumar, and Y. Yu, “Petuum: A new platform for distributed machine learning on big data,” in *Proceedings of the 21th ACM SIGKDD International Conference on Knowledge Discovery and Data Mining*, 2015, pp. 1335–1344.
- [155] Y. Xu, H. Lee, D. Chen, B. Hechtman, Y. Huang, R. Joshi, M. Krikun, D. Lepikhin, A. Ly, and M. Maggioni, “GSPMD: General and scalable parallelization for ML computation graphs,” *arXiv preprint arXiv:2105.04663*, 2021.
- [156] Z. Xu, D. Kong, J. Liu, J. Li, J. Hou, X. Dai, C. Li, S. Wei, Y. Hu, and S. Yin, “WSC-LLM: Efficient LLM service and architecture co-exploration for wafer-scale chips,” in *Proceedings of the 52nd Annual International Symposium on Computer Architecture*, 2025, pp. 1–17.
- [157] Q. Yang, J. Liu, T. Wei, Y. Jin, S. Yin, and Y. Hu, “Segmentation-aware optimization of collective for waferscale chips,” in *International Symposium on Advanced Parallel Processing Technologies*. Springer, 2025, pp. 34–46.
- [158] Q. Yang, T. Wei, S. Guan, C. Li, H. Shang, J. Deng, H. Wang, C. Li, L. Wang, and Y. Zhang, “PD constraint-aware physical/logical topology co-design for network on wafer,” in *Proceedings of the 52nd Annual International Symposium on Computer Architecture*, 2025, pp. 49–64.
- [159] S.-F. Yang, W.-C. Wang, Y.-T. Lin, C.-C. Hung, H.-Y. Tung, and J. Hsieh, “Signal integrity designs at organic interposer CoWoS-R for HBM3-9.2 Gbps high speed interconnection of 2.5 D-IC chipllets integration,” in *2024 IEEE 74th Electronic Components and Technology Conference (ECTC)*. IEEE, 2024, pp. 1098–1103.
- [160] X. Yang, M. Gao, Q. Liu, J. Setter, J. Pu, A. Nayak, S. Bell, K. Cao, H. Ha, and P. Raina, “Interstellar: Using halide’s scheduling language to analyze dnn accelerators,” in *Proceedings of the Twenty-Fifth International Conference on Architectural Support for Programming Languages and Operating Systems*, 2020, pp. 369–383.
- [161] X. Yu, D. Jiang, J. Deng, J. Liu, C. Li, S. Yin, and Y. Hu, “Cramming a data center into one cabinet, a co-exploration of computing and hardware architecture of waferscale chip,” in *Proceedings of the 52nd Annual International Symposium on Computer Architecture*, 2025, pp. 631–645.
- [162] J. Zhai, L. Liao, X. Liu, Y. Wang, R. Li, X. Cao, L. Gao, Z. Gong, F. Gu, and M. He, “Actions speak louder than words: Trillion-parameter sequential transducers for generative recommendations,” *arXiv preprint arXiv:2402.17152*, 2024.
- [163] H. Zhang, A. Ning, R. B. Prabhakar, and D. Wentzlaff, “LLMCompass: Enabling efficient hardware design for large language model inference,” in *2024 ACM/IEEE 51st Annual International Symposium on Computer Architecture (ISCA)*. IEEE, 2024, pp. 1080–1096.
- [164] W. Zhao, B. Lv, M. Wu, P. Chen, F. Yan, Y. Ma, T. Jia, R. Huang, and L. Ye, “3D-TokSIM: Stacking 3D memory with token-stationary compute-in-memory for speculative LLM inference,” in *2025 62nd ACM/IEEE Design Automation Conference (DAC)*. IEEE, 2025, pp. 1–7.
- [165] X. Zhao, J. Zhang, J. Zhang, P. Yuan, H. Jin, and X. Li, “Cooco: A collaborative offloading and resource configuration algorithm in edge networks,” *IEEE Internet of Things Journal*, 2023.
- [166] Y. Zhao, A. Gu, R. Varma, L. Luo, C.-C. Huang, M. Xu, L. Wright, H. Shojanazeri, M. Ott, S. Shleifer, A. Desmaison, C. Balioglu, P. Damania, B. Nguyen, G. Chauhan, Y. Hao, A. Mathews, and S. Li, “PyTorch FSDP: Experiences on Scaling Fully Sharded Data Parallel,” *arXiv preprint arXiv:2304.11277*, 2023.
- [167] L. Zheng, Z. Li, H. Zhang, Y. Zhuang, Z. Chen, Y. Huang, Y. Wang, Y. Xu, D. Zhuo, and E. P. Xing, “Alpa: Automating inter-and intra-operator parallelism for distributed deep learning,” in *16th USENIX Symposium on Operating Systems Design and Implementation (OSDI 22)*, 2022, pp. 559–578.

- [168] Q. Zhou, H. Wang, X. Yu, C. Li, Y. Bai, F. Yan, and Y. Xu, "Mpress: Democratizing billion-scale model training on multi-GPU servers via memory-saving inter-operator parallelism," in *2023 IEEE International Symposium on High-Performance Computer Architecture (HPCA)*. IEEE, 2023, pp. 556–569.
- [169] J. Zhu, C. Xue, Y. Chen, Z. Wang, and G. Sun, "The-seus: Towards high-efficiency wafer-scale chip design space exploration for large language models," *arXiv preprint arXiv:2407.02079*, 2024.
- [170] R. Zong, J. Zhang, Z. Tang, and K. Li, "iBing: An efficient interleaved bidirectional ring all-reduce algorithm for gradient synchronization," *ACM Transactions on Architecture and Code Optimization*, 2025.